Taylor & Francis
Taylor & Francis Group

RESEARCH ARTICLE

Gut microbiota and metabonomics used to explore the mechanism of Qing'e Pills in alleviating osteoporosis

Hui Xie[a,b] (iD), Zhengying Hua[a,b], Mengyu Guo[a,b], Shangyang Lin[a,b], Yaqian Zhou[a,b], Zebin Weng[c], Li Wu[a], Zhipeng Chen[a,b], Zisheng Xu[d] and Weidong Li[a,b]

[a]School of Pharmacy, Nanjing University of Chinese Medicine, Nanjing, China; [b]Jiangsu Key Laboratory of Chinese Medicine Processing, Engineering Center of State Ministry of Education for Standardization of Chinese Medicine Processing, Nanjing University of Chinese Medicine, Nanjing, China; [c]School of Chinese Medicine, Nanjing University of Chinese Medicine, Nanjing, China; [d]Wuhu Pure Sunshine Natural Medicine Company Limited, Wuhu, China

ABSTRACT

Context: The traditional Chinese medicine Qing'e Pills (QEP) has been used to treat postmenopausal osteoporosis (PMO).

Objective: We evaluated the regulatory effects of QEP on gut microbiota in osteoporosis.

Materials and methods: Eighteen female SD rats were divided into three groups: sham surgery (SHAM), ovariectomized (OVX) and ovariectomized treated with QEP (OVX + QEP). Six weeks after ovariectomy, QEP was administered to OVX + QEP rats for eight weeks (4.5 g/kg/day, i.g.). After 14 weeks, the bone microstructure was evaluated. Differences in gut microbiota were analysed via 16S rRNA gene sequencing. Changes in endogenous metabolites were studied using UHPLC-Q-TOF/MS technology. GC–MS was used to detect short-chain fatty acids. Furthermore, we measured serum inflammatory factors, such as IL-6, TNF-α and IFN-γ, which may be related to gut microbiota.

Results: OVX + QEP exhibited increased bone mineral density (0.11 ± 0.03 vs. 0.21 ± 0.02, $p < 0.001$) compared to that of OVX. QEP altered the composition of gut microbiota. We identified 19 potential biomarkers related to osteoporosis. QEP inhibited the elevation of TNF-α (38.86 ± 3.19 vs. 29.43 ± 3.65, $p < 0.05$) and IL-6 (83.38 ± 16.92 vs. 45.26 ± 3.94, $p < 0.05$) levels, while it increased the concentrations of acetic acid (271.95 ± 52.41 vs. 447.73 ± 46.54, $p < 0.001$), propionic acid (28.96 ± 5.73 vs. 53.41 ± 14.26, $p < 0.01$) and butyric acid (24.92 ± 18.97 vs. 67.78 ± 35.68, $p < 0.05$).

Conclusions: These results indicate that QEP has potential of regulating intestinal flora and improving osteoporosis. The combination of anti-osteoporosis drugs and intestinal flora could become a new treatment for osteoporosis.

Introduction

According to the definition of the World Health Organisation (WHO), osteoporosis is a systemic disease characterized by decreased bone mass, destroyed bone microstructure, increased bone brittleness and increased bone fracture tendency. One in two postmenopausal women may have osteoporotic fractures in their lifetime (Shoback et al. 2019). Although oestrogen replacement therapy was the only approved osteoporosis medication, it is not currently recommended because it has shown adverse effects on the heart in elderly women (Saleh et al. 2020). Current medications have also shown side effects. For example, calcitonin can cause bone pain, while tripeptides cannot be used for long periods (Wang et al. 2020). Therefore, the prevention and treatment of postmenopausal osteoporosis (PMO) have attracted worldwide attention in the field of drug research and development.

Qing'e Pills (QEP) is included in the Pharmacopoeia of the People's Republic of China and is a classic prescription for treating osteoporosis (State Pharmacopoeia Committee 2015). QEP is derived from an ancient formula of traditional Chinese medicine (TCM), which is usually used to tonify the kidneys and strengthen bones. Our previous studies revealed that QEP can regulate the balance of bone metabolism. Specifically, QEP promotes bone calcium absorption, regulates calcium and phosphorus balance, inhibits osteoclast activity, stabilizes bone metabolism, promotes osteoblasts, generates bone matrix and restores normal bone metabolism in rats with osteoporosis (Liu et al. 2018; Shuai et al. 2019). However, the underlying mechanisms of action remain unclear.

In recent years, the relationship between intestinal microecology and bone metabolism has emerged as a prevalent topic in medical research, and studies have shown that intestinal flora is related to osteoporosis. Dao et al. (2016) found that injection of oestrogen-inhibiting drugs (imitating menopause in women) caused a significant loss in the bone mass of normal mice, but not in that of sterile mice.

Recent research has shown that the decrease in endogenous oestrogen production caused after ovariectomy alters the composition of intestinal bacteria (Hamm et al. 2019). The

composition and activities of the gut microbiota have developed with the host since birth and are affected by complex interactions between the host's genome, nutrition and lifestyle. Numerous studies have shown that the intestinal microbiota participates in the regulation of various metabolic pathways in mammals through a series of host–microbiota interactions, signal transduction and immune–inflammatory axes. These axes are physiologically connected to the intestine, liver, brain and other organs (Xie et al. 2013). The ecological imbalance of the intestinal microflora increases the abundance of bacteria, which can degrade mucin and inhibit mucin production (Rios-Arce et al. 2017). Decreased mucin activates the NF-κB pathway, which, in epithelial cells, increases pro-inflammatory cytokines, such as TNF-α, IL-1 and IFN-γ. Increased IFN-γ levels can rearrange the actin cytoskeleton. Finally, the integrity of the epithelial layer is destroyed, and intestinal permeability is increased (Rios-Arce et al. 2017). This can lead to increased levels of osteoporosis-related metabolites in blood circulation and the generation of numerous osteoclastogenic factors, such as TNF-α. TNF-α induces the production of RANKL and M-CSF while downregulating osteoprotegerin, thereby promoting osteoclast activation and bone resorption (Pacifici 2012). Short-chain fatty acids (SCFAs) in the intestinal tract, such as acetic acid, propionic acid and butyric acid, are thought to be closely related to osteoporosis. Propionic acid and butyric acid significantly inhibit two essential osteoclast signal transduction components, namely TRAF6 and NFATc1 (Lucas et al. 2018). Butyrates can increase the number of regulatory T cells (Tregs) in the intestine and bone marrow. Tregs can stimulate CD8 + T cells, which can secrete Wnt10b and promote bone formation by activating Wnt signalling in osteoblasts (Tyagi et al. 2018).

QEP contains flavonoids, lignans, proteins, etc. Lignans and flavonoids, which were isolated from QEP, significantly affected the constituents of the gut microbiota (Feng et al. 2014; Zu et al. 2016). Therefore, we hypothesized that the anti-osteoporosis activity of QEP may be due to its function in gut microbiota regulation.

In this study, ovariectomized (OVX) rats were used to evaluate the effect of QEP on osteoporosis. Also, 16s rRNA sequencing analysis was performed to determine changes in the intestinal flora of OVX rats. OVX rats were used to evaluate the effect of QEP on intestinal flora regulation and anti-osteoporosis. In addition, UPLC-Q-TOF/MS-based serum metabolomics analysis and GC-MS-based faecal metabolomics analysis were conducted to better understand the mechanism of the anti-osteoporosis effect of QEP.

Materials and methods

Preparation of QEP

QEP contains four species of traditional Chinese herbs, which are listed in Table 1. The raw materials of the herbs were purchased from Bencao Fangyuan Pharmaceutical Technology Co., Ltd. (Beijing, China).

Table 1. QEP composition.

Chinese name	Latin binomial	Ratio
Du Zhong	Eucommia ulmoides Oliv.	16
Bu Gu Zhi	Psoralea corylifolia Linn.	8
He Tao	Juglans regia L.	5
Da Suan	Allium sativum L.	4

These herbs were identified as the dry bark of *Eucommia ulmoides* Oliv. (Eucommiaceae) and the dry mature fruit of *Psoralea corylifolia* Linn. (Leguminosae) by Professor Chen Jianwei from the School of Pharmacy, Nanjing University of Traditional Chinese Medicine. Both traditional Chinese herbs were processed in our laboratory in accordance with the requirements of the general rules for processing in Appendix IID of the 2020 edition of the Chinese Pharmacopoeia.

The obtained powder (800 g) was weighed, added to 6400 mL of 95% ethanol, heated and refluxed twice for 1 h each time. The alcohol solution was combined, and the residue was added into water of eight times its mass, heated and refluxed twice for 1 h each time. The obtained alcohol and water solutions were combined and concentrated. The final concentration of the extract solution was per millilitre equivalent to 0.45 g of the QEP powder.

Component analysis of QEP

For the analysis of QEP, approximately 2.0 g of powder with 10 times the amount of 95% ethanol was refluxed in a water bath for 1 h and passed through a 0.45 μm microporous membrane as the test solution.

Geniposidic acid, geniposide, pinoresinol diglucoside, psoralenoside, isopsoralenoside, genipin, pinoresinol, psoralen, isopsoralen, isobavachin, neobavaisoflavone, bavachin, bavachalcone, isobavachalcone, bavachinin, corylifol A, 4′-O-methylbroussochalcone and bakuchiol were weighed in appropriate amounts and placed in a brown 5 mL volumetric flask. Methanol was added to dissolve the mixture, which was diluted to volume, shaken well, and prepared to contain 0.453, 0.440, 0.447, 0.240, 0.357, 0.267, 0.240, 0.378, 0.277, 0.280, 0.220, 0.180, 0.237, 0.193, 0.320, 0.096, 0.277 and 2.217 mg/mL of the above compounds, respectively; the mixed stock solution was stored at 4 °C for later use. The calibration curves are listed in Table 2.

A Kromasil 100-5-C18 column (4.6 mm × 250 mm, 5 μm) was used with a mobile phase of 0.1% formic acid water (A)–acetonitrile (B), following the gradient elution program: 0–5 min, 95% (A); 5–35 min, 95–55% (A); 35–60 min, 55–20% (A); 60–75 min, 20–5% (A); 75–85 min, 5–95% (A); 85–87 min, 95–95% (A). The flow rate was 1.0 mL/min, the detection

Table 2. The calibration curves, correlation coefficients (R^2) of reference substance.

Reference substance	Calibration curves	R^2	Liner range (mg/mL)
Geniposidic acid	$Y = 2 \times 10^{-7}X + 0.0037$	0.9998	0.014–0.453
Geniposide	$Y = 7 \times 10^{-8}X + 0.0007$	0.9999	0.014–0.440
Pinoresinol diglucoside	$Y = 2 \times 10^{-7}X - 0.0006$	0.9998	0.014–0.447
Psoralenoside	$Y = 3 \times 10^{-8}X + 0.0001$	0.9999	0.008–0.240
Isopsoralenoside	$Y = 3 \times 10^{-8}X - 0.0006$	0.9997	0.011–0.357
Genipin	$Y = 5 \times 10^{-8}X + 0.0003$	0.9999	0.008–0.267
Pinoresinol	$Y = 2 \times 10^{-7}X + 0.0010$	0.9999	0.008–0.240
Psoralen	$Y = 1 \times 10^{-8}X - 0.0029$	0.9997	0.012–0.378
Isopsoralen	$Y = 1 \times 10^{-8}X + 0.0003$	0.9998	0.009–0.277
Isobavachin	$Y = 6 \times 10^{-8}X - 0.0022$	0.9995	0.009–0.280
neobavaisoflavone	$Y = 2 \times 10^{-8}X - 0.0002$	0.9999	0.007–0.220
Bavachin	$Y = 4 \times 10^{-8}X + 0.0002$	0.9999	0.006–0.180
Bavachalcone	$Y = 5 \times 10^{-8}X - 0.0002$	0.9998	0.007–0.237
Isobavachalcone	$Y = 6 \times 10^{-8}X - 0.0004$	0.9998	0.006–0.193
Bavachinin	$Y = 5 \times 10^{-8}X - 0.0003$	0.9999	0.010–0.320
Corylifol A	$Y = 9 \times 10^{-8}X - 0.0010$	0.9999	0.003–0.096
4′-O-Methylbroussochalcone	$Y = 6 \times 10^{-8}X + 0.0001$	0.9999	0.009–0.277
Bakuchiol	$Y = 6 \times 10^{-8}X + 0.0069$	0.9999	0.069–2.217

wavelengths were 246 nm and 277 nm, the injection volume was 10 μL and the column temperature was 30 °C.

Experiment design

Eighteen female Sprague-Dawley rats, all 3-months-old, were supplied by the Qinglongshan Laboratory Animal Centre (Nanjing, China; certificate no. SCXK-2018-0049). All rats were housed in a specific-pathogen-free environmentally controlled room at a constant temperature (20–24 °C) and humidity (45–60%) and they were supplied with a standard 12 h light/dark cycle for seven successive days before the experiment. This study was approved by the Animal Ethics Committee of Nanjing University of Chinese Medicine (approval number: 202006A005).

Previous research showed that QEP affects osteoporosis (Yan et al. 2014). When exploring new targets, the original dose must be used to ensure that further research is based on curative effects. Therefore, a single dose was used.

The rats were randomly divided into three groups ($n = 6$): (1) control group (SHAM); (2) OVX group, in which ovariectomized rats were treated with saline, and (3) OVX + QEP group, in which ovariectomized rats were treated with a QEP extract solution in accordance with the clinically converted dose (4.5 g/kg/day, i.g.). After one week of adaptive feeding, all animals in the three groups underwent surgery. Either ovariectomy or sham surgery was performed under intraperitoneal anaesthesia with pentobarbital (40 mg/kg). In OVX rats, the bilateral ovaries were excised via back incisions, while the equivalent weight of adipose tissue was excised from SHAM rats. Six weeks after the operation, QEP was administered to the rats in the OVX + QEP group daily for eight weeks. The samples were prepared on the last day of drug administration (Figure 1).

Faecal sample collection

After 12 weeks of administration, fresh stool samples from rats in each group were taken using the abdominal compression method. Two parallel faecal samples were collected from each rat in sterile containers and immediately frozen at −80 °C.

Organs and serum collection

At the end of the trial, the rats were fasted for 8 h and then anaesthetized with sodium pentobarbital (the concentration was controlled at 70 mg/kg). The rats were sacrificed after blood was collected from the heart. Serum was obtained by centrifuging the blood sample at 3500 rpm (4 °C) for 15 min. The right femurs of the rats were dissected, removed, fixed in 10% neutral buffered formalin, washed and stored in PBS at 4 °C. Their uteruses were weighed and stored at −80 °C. From each rat, 2 cm of ileum was removed and washed with PBS; 1 cm of it was directly frozen at −80 °C and the remaining part was fixed in 10% neutral buffered formalin.

Bone mineral density and microarchitecture measurement

The collected femur samples were independently fixed in cuboid moulds made of silicone rubber. The distal femur was scanned using a micro-CT (Skyscan 1176, Bruker, Kontich, Belgium). The scanning voltage, current and layer thickness were set as 65 kV, 385 μA and 18 μm, respectively.

The data obtained from the micro-CT scan were imported into NRecon v.1.6.3 (Bruker micro CT, Kontich, Belgium) for 3D reconstruction and were then quantitatively analysed using CTAn and CTvol. The following parameters were obtained: bone mineral density (BMD, g/cm^3), bone volume fraction (BV/TV, %), bone surface density (BS/TV, mm^{-1}), trabecular number (Tb.N, mm^{-1}) and trabecular separation (Tb.Sp, mm).

Determination of biochemical indicators

The collected plasma samples were removed from the refrigerator at −80 °C and thawed at 4 °C. The rat bone-specific alkaline phosphatase (BAP) and anti-tartrate acid phosphatase (TRAP) ELISA test kits were used for detection.

Gut microbiota analysis

DNA from the intestinal microbial community was extracted from the faecal samples using the E.Z.N.A.® DNA Kit (Omega Bio-tek, Norcross, GA) in accordance with the manufacturer's instructions. The hypervariable regions V3–V4 of the bacterial 16S rRNA gene were amplified using an ABI GeneAmp® 9700 polymerase chain reaction (PCR) thermocycler (ABI, Foster City, CA). The PCRs were performed in triplicate; the product was extracted from a 2% agarose gel and purified using the AxyPrep DNA Gel Extraction Kit (Axygen Biosciences, Union City, CA)

Table 3. The calibration curves, correlation coefficients (R^2) of SCFAs.

SCFAs	Calibration curves	R^2	Liner range (μg/mL)
Acetate	$y = 0.0002x - 13.353$	$R^2 = 0.9995$	750–23.44
Propionate	$y = 6E{-}05x - 2.784$	$R^2 = 0.9998$	750–23.44
Butyrate	$y = 7E{-}05x + 1.1839$	$R^2 = 0.9997$	375–11.72
Isobutyrate	$y = 0.0002x - 2.1728$	$R^2 = 0.9990$	93.75–2.93
Valerate	$y = 8E{-}05x + 3.867$	$R^2 = 0.9993$	93.75–2.93
Isovalerate	$y = 7E{-}05x - 0.6331$	$R^2 = 0.9995$	93.75–2.93

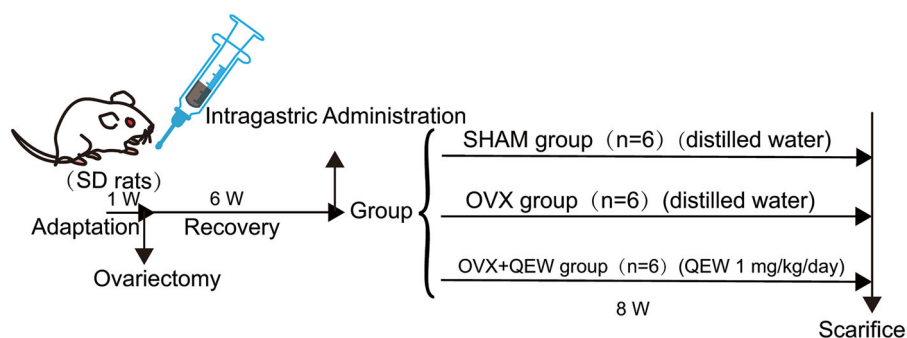Figure 1. Animal experimental design.

in accordance with the manufacturer's instructions and quantified using a Quantus™ Fluorometer (Promega, Madison, WI).

The purified amplicons were pooled in equimolar concentrations and paired-end sequenced (2 × 300) on an Illumina MiSeq platform (Illumina, San Diego, CA) in accordance with the standard protocols of Majorbio Bio-Pharm Technology Co. Ltd. (Shanghai, China). The raw 16S rRNA gene sequencing reads were demultiplexed, quality-filtered using Trimmomatic, and merged using FLASH.

Operational taxonomic units (OTUs) with 97% similarity cutoff were clustered using UPARSE (version 7.1, http://drive5.com/uparse/), and chimeric sequences were identified and removed. The taxonomy of each OTU representative sequence was analysed using the RDP Classifier (http://rdp.cme.msu.edu/) against the 16S rRNA database with a confidence threshold of 0.7.

Analysis of endogenous metabolism in rat plasma

The collected plasma samples were removed from the refrigerator at −80 °C and thawed at 4 °C. Each plasma sample (100 μL) was added to 300 μL of methanol to precipitate the protein, vortexed for 5 min, and centrifuged twice (12,000 rpm, 5 min). The supernatant (200 μL) was used for the UPLC-Q/TOF-MS analysis.

The mobile phase consisted of 0.1% formic acid aqueous solution (A) and acetonitrile (B), and the gradient elution settings were the following: 0.1–0.2 min, 95% (A)–90% (A), 0.2–0.5 min, 90% (A)–90% (A), 0.5–4 min, 90% (A)–60% (A), 4–9 min, 60% (A)–47% (A), 9–17 min, 47% (A)–20% (A), 17–25 min, 20% (A)–0% (A). The flow rate was 0.3 mL/min, the column temperature was 35 °C, and the injection volume was 1 μL. The chromatographic column used was an Agilent C_{18} (2.1 mm × 100 mm, 1.8 μm) column.

The scanning mode of mass spectrometry was carried out separately for the positive and negative ions. The instrument parameters were as follows: spray auxiliary gas: atomizing gas (gas 1): 55 psi; auxiliary heater (gas 2): 55 psi; curtain gas: 35 psi; ion source temperature: 550 °C; ion spray voltage: 4500 V/−4500 V; declustering potential: 60 V/−60 V; collision energy: 35 V/−35 V; TOF-MS scanning range: 100–2000 Da; and production MS scan range: 50–1500 Da.

The raw data collected via UPLC-Q/TOF-MS were used to align and normalize the chromatographic peaks using the MarkView™ software. The retention time range was 1–32 min, the mass scan range was 100–1000 Da, the mass tolerance range was 0.05 Da, and the peak intensity threshold was 100. The extracted ion intensities were normalized using the total peak area method. Standard data were imported into SIMICA14.0 for further mathematical model analysis. The partial least squares and orthogonal partial least squares discriminants were used to analyse the dispersion degree of the data and obtain the variable importance in projection (VIP) value. The rate-corrected t-test was used to measure the significance of each metabolite, and the p value was obtained; the metabolites with VIP > 1 and $p < 0.05$ were defined as differential metabolites.

Based on the information of the mass-to-charge ratio (m/z) in the public databases HMDB and KEGG, the obtained metabolic difference substances were identified and confirmed with the isotope matching rate and secondary fragment matching rate provided by the PeakView software. The screened endogenous metabolites were submitted to Metabo Analyst for correlation analysis of metabolic pathways.

Table 4. QEP content analysis.

| Reference substance	Content
Geniposidic acid	0.064 ± 0.002
Geniposide	0.013 ± 0.000
Pinoresinol diglucoside	0.067 ± 0.003
Psoralenoside	0.246 ± 0.005
Isopsoralenoside	0.172 ± 0.004
Genipin	0.014 ± 0.000
Pinoresinol	0.043 ± 0.007
Psoralen	0.119 ± 0.004
Isopsoralen	0.101 ± 0.002
Isobavachin	0.030 ± 0.001
Neobavaisoflavone	0.080 ± 0.002
Bavachin	0.037 ± 0.001
Bavachalcone	0.103 ± 0.002
Isobavachalcone	0.084 ± 0.002
Bavachinin	0.103 ± 0.002
Corylifol A	0.217 ± 0.006
4′-O-Methylbroussochalcone	0.065 ± 0.001
Bakuchiol	1.366 ± 0.031
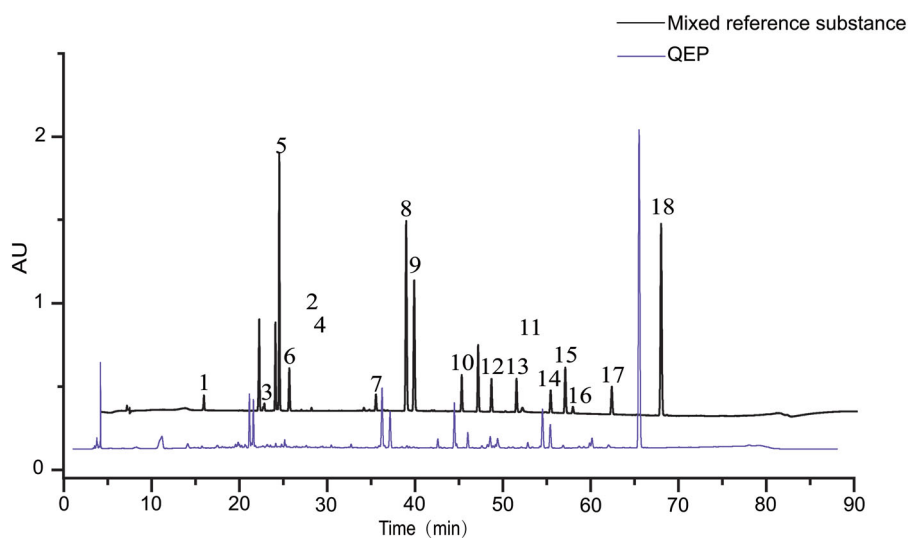
Figure 2. HPLC chromatogram of QEP. (1) Geniposidic acid; (2) geniposide; (3) pinoresinol diglucoside; (4) psoralenoside; (5) isopsoralenoside; (6) genipin; (7) pinoresinol; (8) psoralen; (9) isopsoralen; (10) isobavachin; (11) neobavaisoflavone; (12) bavachin; (13) bavachalcone; (14) isobavachalcone; (15) bavachinin; (16) corylifol A; (17) 4′-O-methylbroussochalcone; (18) bakuchiol.
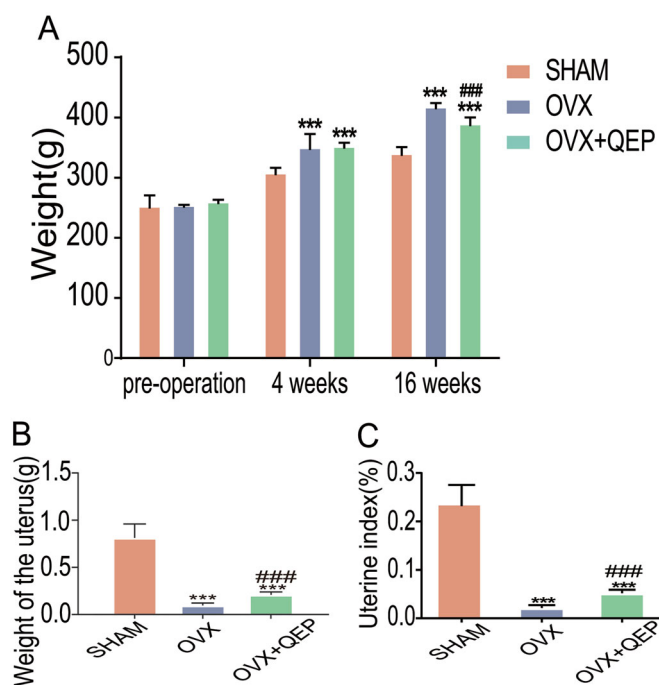
Figure 3. Effects of QEP on body weight, uterine weight and uterine index. Comparison of (A) body weight, (B) uterine weight and (C) uterine index levels among the groups at 12 weeks post-operation. The data are expressed as means ± SD ($n = 6$ in each group). ***$p < 0.001$ vs. SHAM. ###$p < 0.001$ vs. OVX.

Quantification of serum TNF-α, IL-6 and IFN-γ, and histopathology analysis

Frozen stored serum samples were removed and thawed at room temperature and centrifuged at $1600 \times g$ for 15 min at 4 °C. Inflammatory factors were detected using TNF-α, IL-6 and IFN-γ ELISA kits (Multi Sciences, Hangzhou, China), in accordance with the manufacturer's instructions.

The excised tissue from the ileum was rapidly cleaned and fixed in 4% paraformaldehyde at 4 °C for 24 h. After embedding in paraffin, blocks were cut into 4 μm thick slices using a rotary microtome (RM2016, Leica, Wetzlar, Germany) and stained with H&E. Finally, each slice was examined under a light microscope (BX51T-PHD-J11, Olympus, Tokyo, Japan) to evaluate the histopathological changes in the ileum.

SCFAs contents measurement

Solutions of the mixed standards were prepared using gradient dilution. Acetic acid and propionic acid were diluted from 750 μg/mL, butyric acid was diluted from 375 μg/mL, and isobutyric acid, isovaleric acid and valeric acid were diluted from 93.75 μg/mL. Moreover, 0.5 mL of each mixed standard was transferred into a 10 mL glass centrifuge tube. Then, 300 μL of water, 300 μL isopropanol/pyridine (3/1 v/v) and 50 μL propyl chloroformate were added to the tube for derivatization. Then, each tube was vortexed and ultrasonicated for 1 min, and 300 μL of n-hexane was added to extract SCFAs. After vortexing for 1 min, the glass centrifuge tubes were centrifuged at 2000 rpm for 10 min. From each tube, 200 μL of supernatant was transferred into a 1.5 mL Eppendorf tube. Another 200 μL of n-hexane was added to each tube for the second extraction step. Finally, 400 μL of the supernatant was injected into the GC–MS system for analysis.

Frozen stored faecal samples were removed and thawed at room temperature. Each faecal sample was mixed with 1 mL of 0.005 M NaOH. The mixture was oscillated for 20 min for complete dispersion and centrifuged at 13,000 rpm for 10 min. The sample preparation procedure was the same as that for the standard solution preparation.

The SCFAs were separated using an Agilent HP-5ms (19091s-433) column (0.25 mm × 30 m × 0.25 μm) with a split ratio of 50:1. The injection volume was 1 μL. The gradient heating program was set as follows: 0–2 min, 50–50 °C; 2–4 min, 50–70 °C; 4–9 min, 70–80 °C; 9–22.5 min, 80–290 °C. Helium (99.999%) was used as the carrier gas, with a flow rate of 1.2 mL/min. The ionization energy was 70 eV, the source temperature was 230 °C, and the quadrupole temperature was 150 °C. The inlet temperature was 250 °C. The GC–MS data were obtained after a solvent delay of 1.50 min. The MS scan range was 40–550 m/z. The calibration curves are listed in Table 3.

Statistical analysis

One-way analysis of variance was performed to investigate alterations among three or more groups, and Student's t-tests were performed to compare the data between only two groups. All statistical analyses were conducted with SPSS 23.0 (SPSS Inc., Chicago, IL) and are expressed as means ± SD. The figures were created using GraphPad Prism 7.0 software (La Jolla, CA). Statistical significance was set at $p < 0.05$. To observe the association between the top 30 most abundant gut microbiota and biomarkers, Spearman's correlation coefficient was established using SPSS 23.0 (SPSS Inc., Chicago, IL).

Results

Component analysis of QEP

We analysed the content of QEP. Eighteen chemical components were identified in QEP, namely, geniposidic acid, geniposide, pinoresinol diglucoside, psoralenoside, isopsoralenoside, genipin, pinoresinol, psoralen, isopsoralen, isobavachin, neobavaisoflavone, bavachin, bavachalcone, isobavachalcone, bavachinin, 4′-O-methylbroussochalcone, corylifol A and bakuchiol, which are often used as active ingredients (Figure 2). The content determination of the 18 components is presented in Table 4.

QEP alleviated osteoporosis in ovariectomized rats

To mimic osteoporosis in the clinic, we constructed a pathological model using ovariectomized female rats. We found that OVX rats gained more weight than rats in the SHAM group (Figure 3(A)). The uterine weight and uterine index of the rats in the OVX group were significantly lower than those of the rats in the SHAM group (Figure 3(B,C)). After treatment with QEP, the bodyweight of the rats in the OVX + QEW group was reduced compared to that of the rats in the OVX group, while the uterine index significantly increased.

To examine the changes in the microstructure of femurs in the OVX rats and the protective effect of QEP, micro-CT was employed to analyse bone morphometric parameters in the femurs of various groups of rats. CTan software was used for the 3D reconstruction of bone microstructures to reflect changes within bone microstructures (Figure 4(A–C)). The coronal plane of the rat femurs was observed directly. The results reflect the internal structure of the bone trabecula (Figure 4(D–F)). The
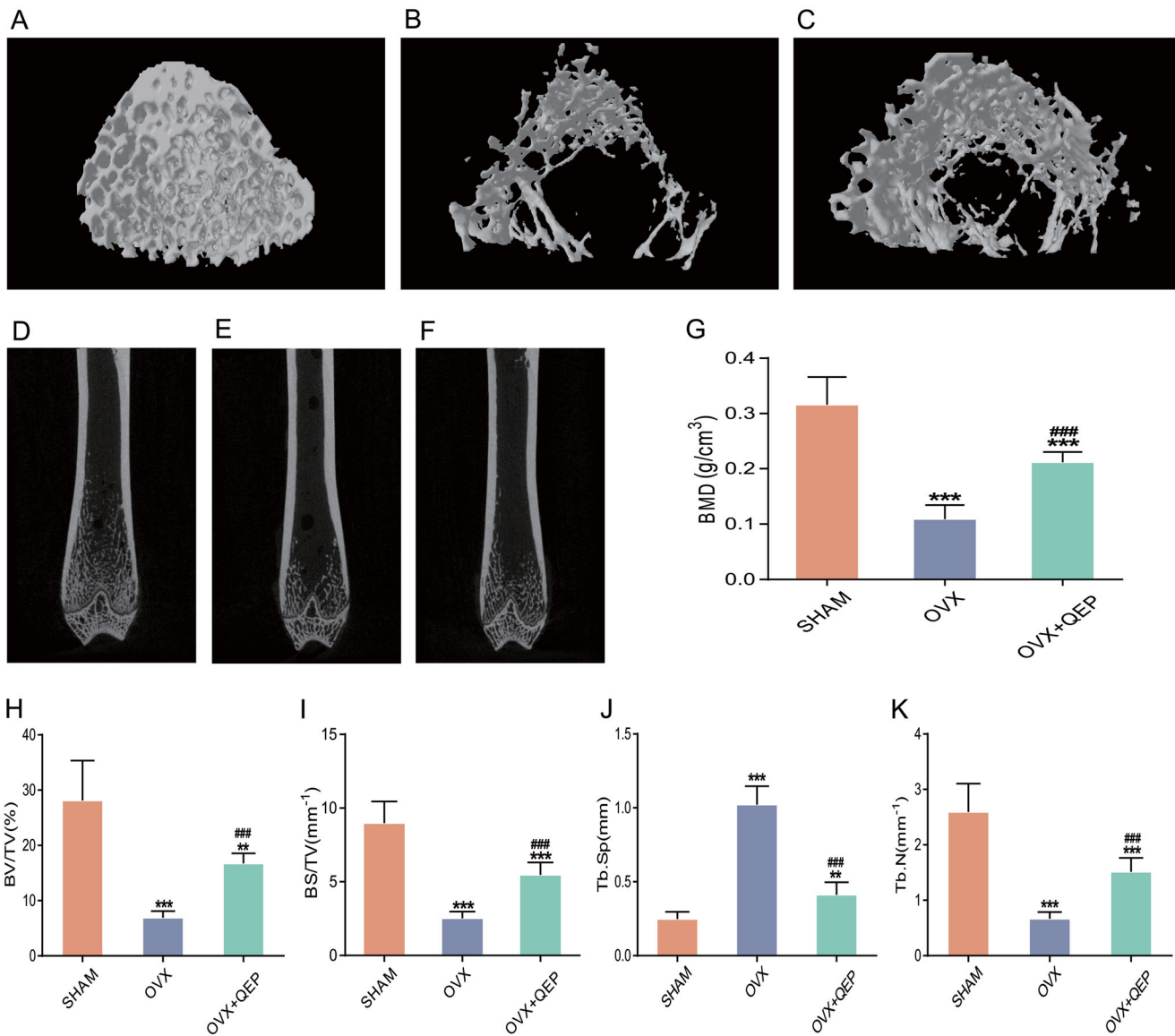
Figure 4. QEP improved bone mass and bone microstructure in OVX rats. (A–C) Representative micro-CT images of femur. (D–F) Coronal view of the distal femur (G–K) Comparison of the BMD, BV/TV, BS/TV, Tb.Sp and Tb.N among the groups. The data are expressed as means ± SD ($n = 6$ in each group). $**p < 0.01$; $***p < 0.001$ vs. SHAM; $###p < 0.001$ vs. OVX.

Table 5. Determination of serum indices.

	SHAM	OVX	QEP
E2	49.26 ± 7.20	$29.90 \pm 3.97^{***}$	$49.52 \pm 6.00^{###}$
BAP	13.21 ± 1.30	$18.18 \pm 0.41^{***}$	$14.29 \pm 1.69^{###}$
BGP	5.35 ± 1.45	$9.44 \pm 1.27^{***}$	$6.67 \pm 0.55^{###}$
TRAP	39.73 ± 7.53	$61.67 \pm 5.55^{***}$	$45.56 \pm 9.58^{##}$

$***p < 0.001$ vs. SHAM; $##p < 0.01$ vs. OVX; $###p < 0.001$.

removal of ovaries can lead to significant bone loss in the femur, which was reflected by decreased BMD, bone volume (BV)/total volume (TV), bone surface area (BS)/tissue volume (TV) and trabecular number (Tb.N), but increased trabecular separation (Tb.Sp). QEP treatment significantly reduced bone loss in OVX rats (Figure 4(G–K)).

Determination of serum indices

As shown in Table 5, the E2 content in the QEP rat serum of the model group was significantly reduced compared with that of the SHAM group but significantly increased compared with that of the OVX group. The serum levels of TRAP, BAP and BGP in the OVX group were significantly higher than those in the SHAM group.

QEP increased the richness and diversity of the gut microbiota community in OVX rats

The intestinal microbial communities in the OVX and OVX + QEP groups were examined. A principal coordinates analysis with weighted and unweighted UniFrac distances was performed to evaluate the microbial community structure (β-diversity) under the three conditions. Both unweighted and weighted UniFrac metrics showed separation in the gut bacterial structure among the three groups. This result suggested that ovariectomy and QEP treatment are key factors affecting the gut microbiota (Figure 5(A,B)). The Shannon diversity index (Figure 5(C)) and the Simpson index (Figure 5(D)) were derived. The overall microbial assortments in the OVX group were significantly higher than those in the SHAM group. In contrast, QEP
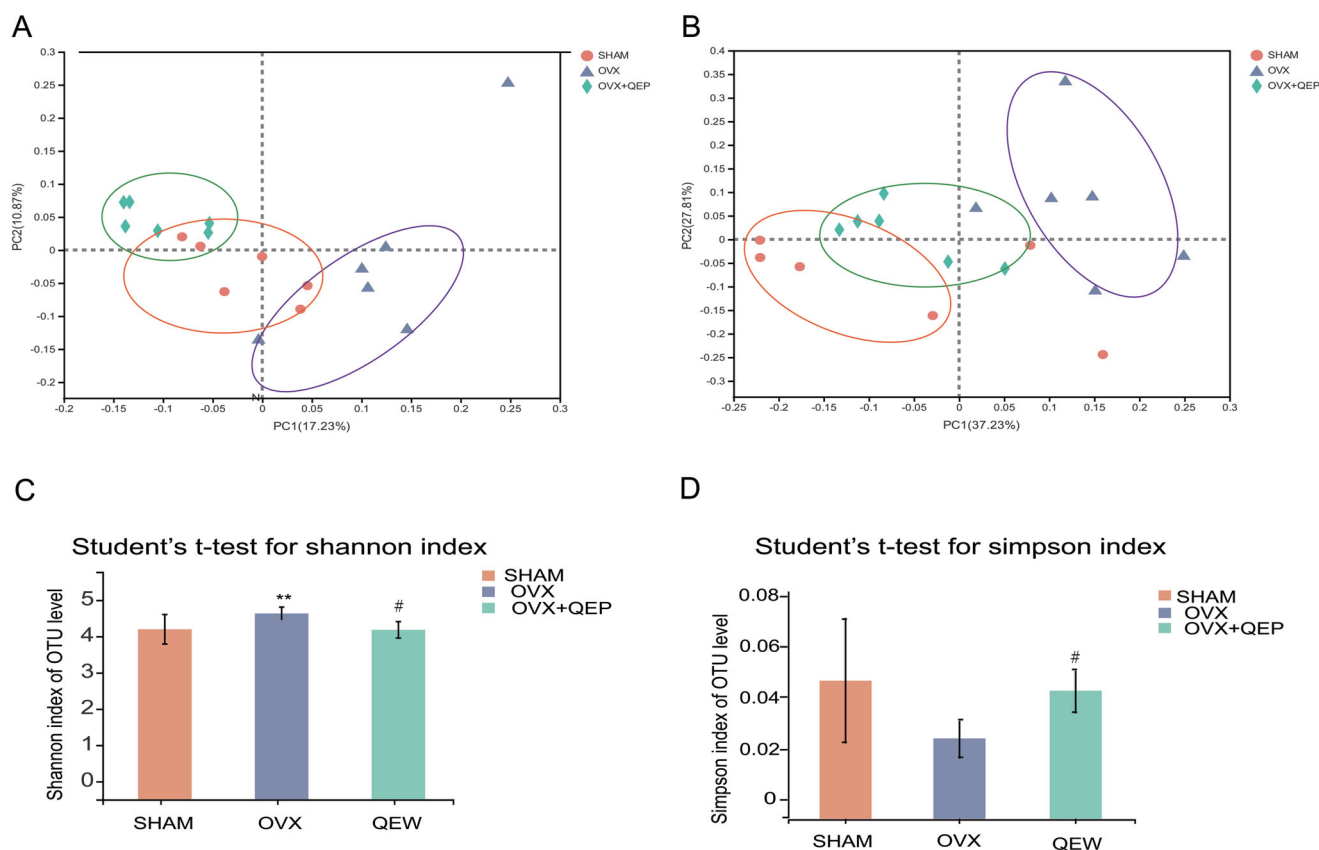
Figure 5. QEP modulated the microbial diversity in OVX rats. (A) Principal coordinates analysis (PCoA) based on an unweighted UniFrac between the groups. (B) PCoA based on a weighted UniFrac between the groups. (C) Shannon diversity index. (D) Simpson diversity index. $**p < 0.01$; $^{\#}p < 0.05$.

treatment significantly prevented an increase in the Shannon and Simpson diversity indexes.

QEP altered composition of gut microbiota in OVX rats

The microbial taxonomic compositions at the phylum and genus levels are presented in Figure 5(A,B). At the phylum level (Figure 6(A)), Firmicutes, Bacteroidetes and Verrucomicrobia were the three predominant phyla in all three groups. The abundance of Firmicutes in the SHAM and OVX groups was 52.5% and 65.97%, that of Bacteroidetes was 31.07% and 29.05%, and that of Verrucomicrobia was 12.97% and 2.37%, respectively. The Firmicutes/Bacteroidetes (F/B) ratio of the SHAM group was 1.69, whereas that of the OVX group was 2.97. The abundance of Firmicutes in the OVX + QEP group was 61.9%, which was lower than that in the OVX group. The abundance of Verrucomicrobia in the OVX + QEP group was 10.14%, which was greater than that in the OVX group. This resulted in a lower F/B ratio in the OVX + QEP group (2.56) compared with that in the OVX group. At the genus level (Figure 6(B)), norank f-Muribaculaceae, *Lactobacillus*, *Akkermansia*, Ruminococcaceae UCG-014 and unclassified f-Lachnospiraceae were the five predominant genera in all groups. The microbial differences at the phylum and genus levels are shown in Figure 6(C,D). The proportion of Firmicutes and Verrucomicrobia in the OVX group changed significantly compared with that in the SHAM group. Furthermore, the constituents of the rat intestinal microbial community in the OVX + QEP group changed significantly compared with those in the OVX group but were similar to those in the SHAM group (Figure 6(C)). At the genus level, the contents of *Lactobacillus* and *Akkermansia* in the OVX group were lower

than those in the SHAM group, whereas the contents of unclassified f-Lachnospiraceae, *Blautia* and Christensenellaceae R-7 group increased (Figure 6(D)). To reveal the relationship between gut microbiota and certain physical signs, such as BMD, BV/TV, BS/TV, Tb.Sp and Tb.N, we calculated Spearman's correlation coefficient of the top 30 most abundant families of the gut microbiome community and these biological indicators. *Lactobacillus* and *Akkermansia* were positively correlated with BMD, BV/TV, BS/TV and Tb.N, but negatively correlated with Tb.Sp (Figure 6(E)). Thus, *Lactobacillus* and *Akkermansia* are beneficial for the prevention and treatment of osteoporosis.

QEP improves related metabolic pathways in the intestinal microbiota

PICRUSt analysis was performed to predict and differentiate gut microbial metabolic function among the three groups, namely SHAM, OVX and OVX + QEP, based on the KEGG database. To examine the regulatory activity of QEP on the gut microbial community of OVX rats, we compared the differences in microbial metabolic functions between the SHAM, OVX and OVX + QEP groups. Comparing the SHAM and OVX groups, we found that multiple KEGG (level 3) categories were disturbed (Figure 7(A)). Some of the KEGG categories (level 3) were adjusted to normal when treated with QEP (Figure 7(B)). QEP can regulate the biosynthesis of amino acids ($p < 0.05$) and the pentose phosphate pathway. In addition, QEP can regulate the metabolism of alanine, aspartic acid, glutamic acid, etc. The metabolism of butanoate and propanoate and the biosynthesis of fatty acids in the intestinal environment of OVX rats can be adjusted to normal levels after treatment with QEP.

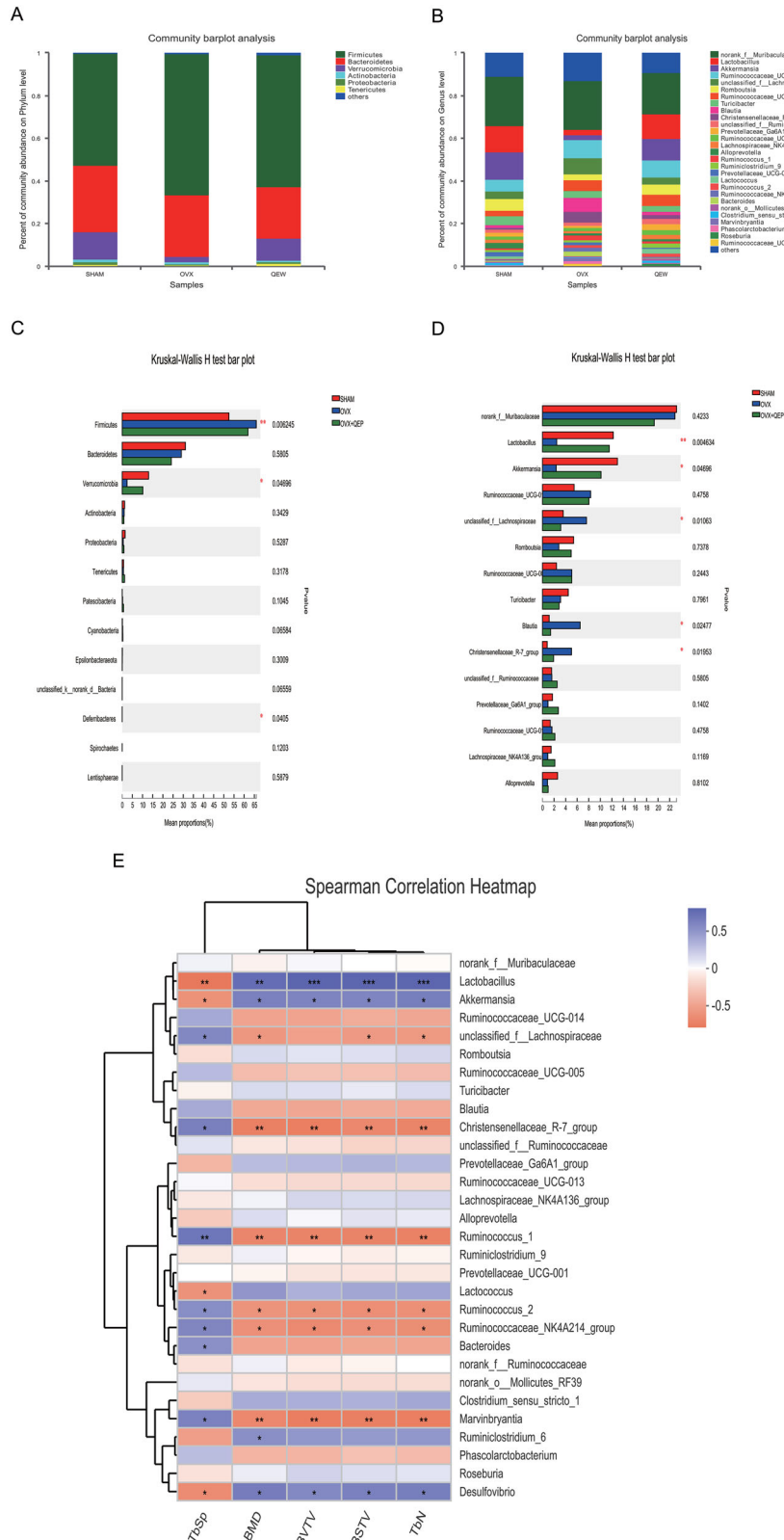**Figure 6.** QEP antagonist changed the gut microflora community composition in OVX rats. Composition of gut microbiota at the (A) phylum and (B) genus levels. Differences in intestinal flora at the (C) phylum and (D) genus levels. (E) Spearman's correlation of the top 30 most abundant families with biomarkers. The data are expressed as means ± SD ($n = 6$ in each group). *$p < 0.05$; **$p < 0.01$; ***$p < 0.001$; vs. SHAM.
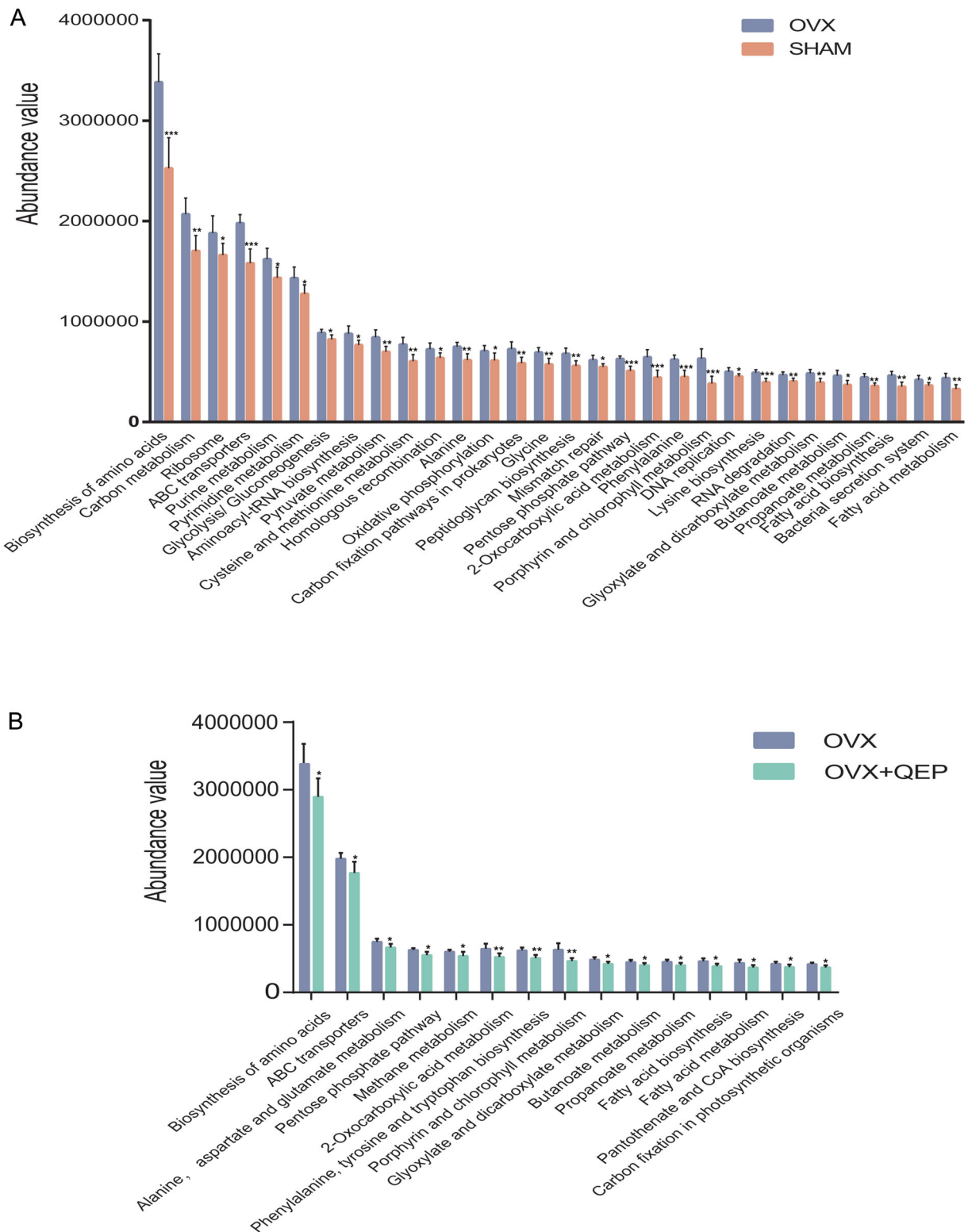
Figure 7. PICRUSt analysis based on KEGG database used to predict microbial metabolic function and analyse the functional differences. Differences between OVX and (A) SHAM and (B) OVX + QEP groups. $*p < 0.05$; $**p < 0.01$; $***p < 0.001$.

Analysis of Qing'e Pills intervening rat plasma endogenous metabolism

The plasma of rats in the sham operation group and osteoporosis model rats was detected via UPLC-Q/TOF-MS to obtain mass spectrometry total ion currents in positive and negative modes, as shown in Figure 8. Figure 8(A–C) shows the total ion currents

of the sham operation group, model group and QEP group in positive ion mode; Figure 8(D–F) shows the total ion currents of the sham operation group, model group and QEP group in negative ion mode.

To reduce the random error within the group, we highlighted the contour difference between the groups, and compensated for the defects of the unsupervised model; the supervised OPLS-DA

Figure 8. Mass spectrometry total ion currents in positive and negative modes. Total ion current of SHAM, OVX and OVX + QEP groups in positive (a, b and c, respectively) and negative (d, e and f, respectively) ion modes.

analysis is used to establish a discriminant model and predict the prediction set. Figure 9 shows the OPLS-DA distribution diagrams, VIP score diagrams and S-plot diagrams of the sham and model groups in the positive (A, B and C, respective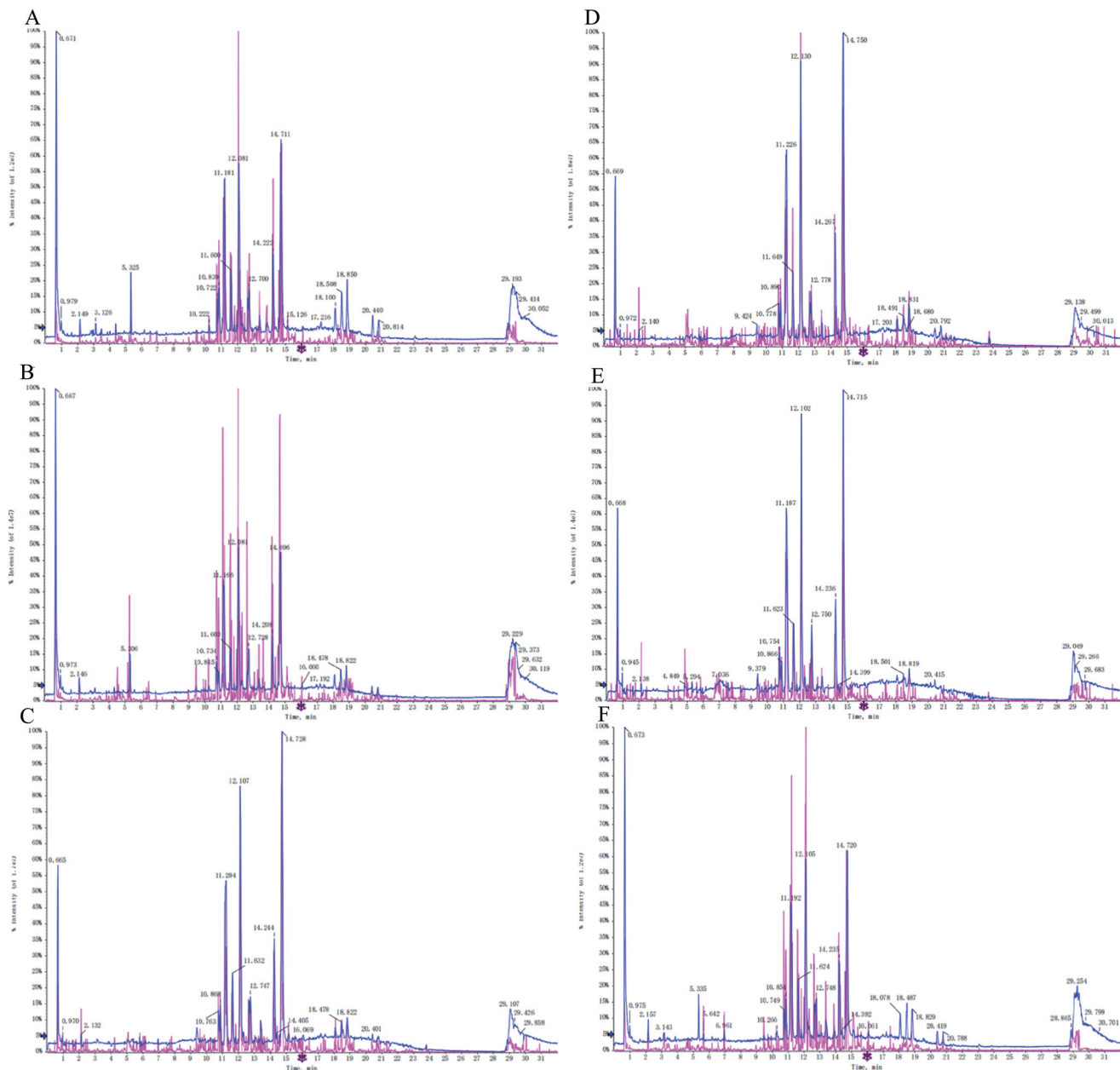ly) and negative (D, E and F, respectively) ion modes. For the positive ion mode, R2[X] = 0.794 and Q2 = 0.982, whereas, for the negative ion mode, R2[X] = 0.935 and Q2 = 0.933, which indicates that the model was reliable. The VIP score graph and S-plot graph show the components that contribute more to the two groups (VIP > 1), combined with $p < 0.05$, in the MarkView data; 262 possible differences were screened out in the positive ion mode, while 274 possible components were screened in the negative ion mode.

The mass-to-charge ratios of the selected components were entered into the online database (https://hmdb.ca/) for comparison. The screening error range was less than 10 ppm. In the positive and negative ion modes, 97 and 44 eligible compounds were screened out, respectively; then, they were combined with the secondary fragments and matching values in the PeakView software, and they were analysed and identified. A total of 44 and 29 differential metabolites were identified in the positive and negative ion modes, respectively; the results are shown in Tables 6 and 7.

The identified potential biomarkers were entered into the online database Metabo Analyst 5.0 (https://www.metaboanalyst. ca/), and the metabolic pathways were further analysed. Nineteen different endogenous metabolites were found in the plasma of osteoporosis model rats, as shown in Table 8. The PeakView software was used to compare and analyse the response values of different endogenous metabolites in each group, and the results
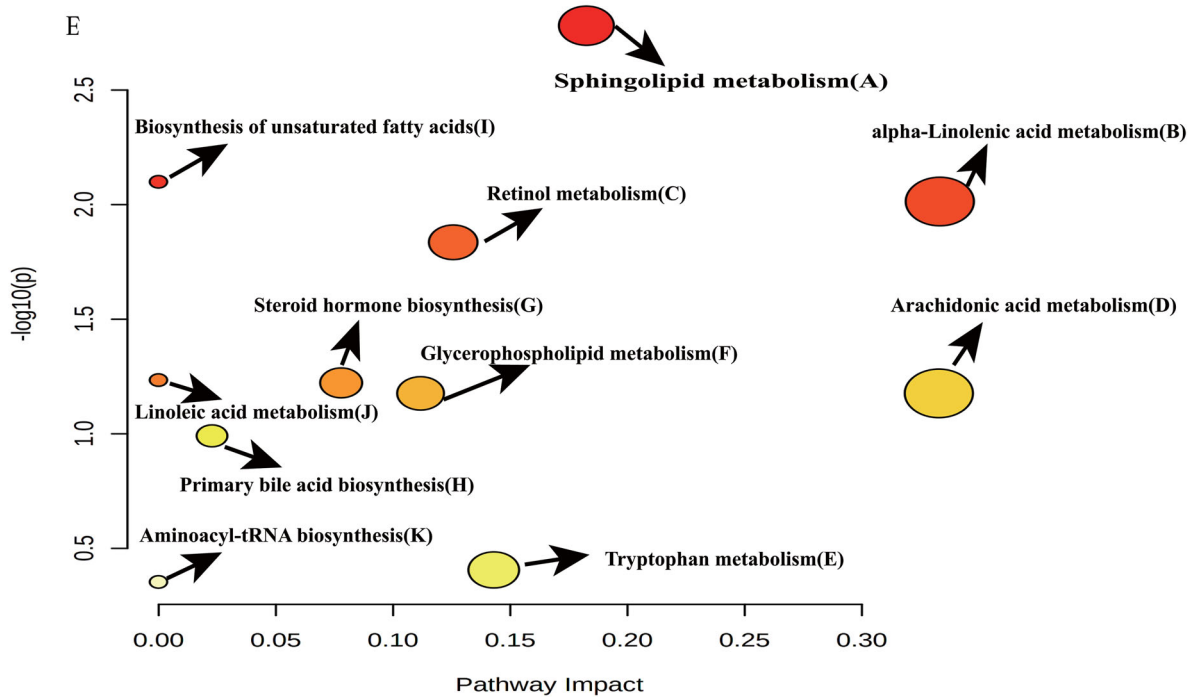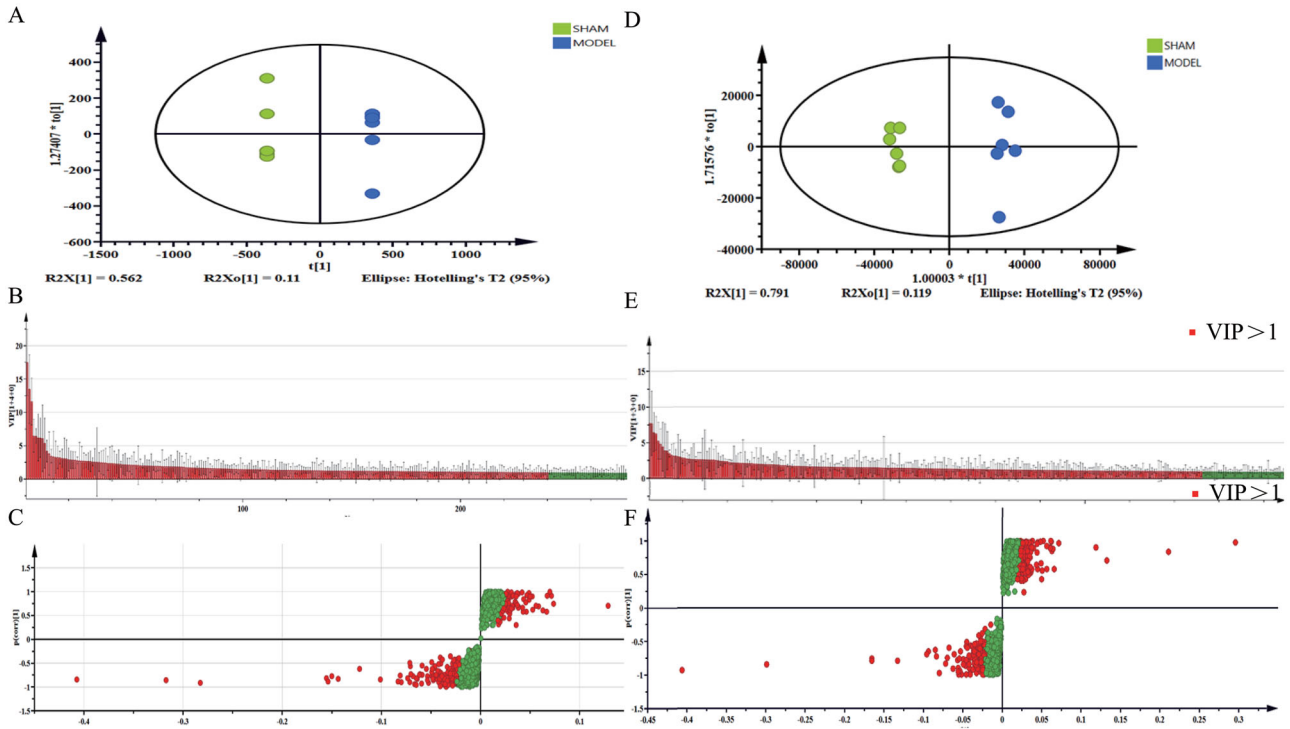
Figure 9. OPLS-DA and metabolic pathway analyses. OPLS-DA distribution diagram, VIP score diagram and S-plot diagram of SHAM and OVX groups in positive (a, b and c, respectively) and negative (d, e and f, respectively) ion modes. (g) Diagram of the main metabolic pathways of potential biomarkers of osteoporosis.

are shown in Table 9. It mainly involves 11 metabolic pathways, including the pathways of unsaturated fatty acid biosynthesis, glycerophospholipid metabolism, linoleic acid metabolism, arachidonic acid metabolism, α-linolenic acid metabolism, primary bile acid biosynthesis, sphingolipid metabolism, tRNA biosynthesis and retinol metabolism (Figure 9(G)).

Quantification of serum TNF-α, IL-6 and IFN-γ, and histopathology analysis

More mucosal epithelia were observed in the OVX group than in the SHAM group. Glands were deformed and atrophied, or structures severely vanished in the gut mucosal epithelia of OVX rats. Submucosal oedema and inflammatory cell infiltration were

Table 6. Identification results of endogenous metabolites in rat plasma that are meaningful for grouping under positive ion mode.

No.	Database ID	Identification	Retention	Formula	Adduct	Extract mass	Delta (ppm)	Matching rate
1	HMDB0013817	2-Benzylheptanoic acid	2.95	$C_{14}H_{20}O_2$	M + H	221.1533	1	100.0
2	HMDB0033072	(E)-1-Propenyl 1-(propylthio)propyl disulphide	9.66	$C_9H_{18}S_3$	M + H	223.0629	6	93.0
3	HMDB0033041	1-(1-Propenylthio)propyl propyl disulphide	10.64	$C_9H_{18}S_3$	M + H	223.0629	6	93.0
4	HMDB0029668	1-(4-Methoxyphenyl)-4-methylpentan-3-ol	6.53	$C_{13}H_{20}O_2$	M + NH4	226.1817	7	88.3
5	HMDB0034495	6,10,14-Trimethyl-5,9,13-pentadecatrien-2-one	18.79	$C_{18}H_{30}O$	M + H	263.2375	2	95.7
6	HMDB0015522	Sulfamethazine	8.12	$C_{12}H_{14}N_4O_2S$	M + H	279.0926	6	93.0
7	HMDB0033244	Dibutyl phthalate	21.44	$C_{16}H_{22}O_4$	M + H	279.1587	1	100.0
8	HMDB0001388	Alpha-linolenic acid	17.21	$C_{18}H_{30}O_2$	M + H	279.2344	9	98.6
9	HMDB0031097	9E,11E-Octadecadienoic acid	18.83	$C_{18}H_{32}O_2$	M + H	281.2481	2	80.3
10	HMDB0002117	Oleamide	18.44	$C_{18}H_{35}NO$	M + H	282.281	7	83.1
11	HMDB0006216	11-cis-Retinol	18.47	$C_{20}H_{30}O$	M + H	287.2368	0	97.6
12	HMDB0000269	Sphinganine	7.55	$C_{18}H_{39}NO_2$	M + H	302.308	9	100.0
13	HMDB0001043	Arachidonic acid	18.49	$C_{20}H_{32}O_2$	M + H	305.2482	2	85.5
14	HMDB0002925	Dihomo-gamma-linolenic acid	19.62	$C_{20}H_{34}O_2$	M + H	307.2641	3	91.8
15	HMDB0032147	Geranylcitronellol	21.16	$C_{20}H_{36}O$	M + NH4	310.3122	6	84.0
16	HMDB0004610	Phytosphingosine	5.93	$C_{18}H_{39}NO_3$	M + H	318.3023	6	100.0
17	HMDB0034780	Capsiate	2.2	$C_{18}H_{26}O_4$	M + NH4	324.2184	5	95.5
18	HMDB0002183	Docosahexaenoic acid	18.08	$C_{22}H_{32}O_2$	M + H	329.2479	1	80.3
19	HMDB0006528	Docosapentaenoic acid (22n-3)	18.89	$C_{22}H_{34}O_2$	M + H	331.2634	1	89.0
20	HMDB0011564	MG(16:0/0:0/0:0)	18.57	$C_{19}H_{38}O_4$	M + H	331.2864	6	100.0
21	HMDB0000363	17a-Hydroxypregnenolone	7.56	$C_{21}H_{32}O_3$	M + H	333.2442	5	91.6
22	HMDB0002226	Adrenic acid	20.43	$C_{22}H_{36}O_2$	M + H	333.2805	5	90.0
23	HMDB0032476	Polyoxyethylene (600) monoricinoleate	21.47	$C_{21}H_{40}O_3$	M + H	341.3073	7	99.0
24	HMDB0001547	Corticosterone	5.6	$C_{21}H_{30}O_4$	M + H	347.222	1	96.7
25	HMDB0002007	Tetracosahexaenoic acid	9.72	$C_{24}H_{36}O_2$	M + H	357.2805	5	94.5
26	HMDB0013025	6,9,12,15,18,21-Tetracosahexaenoic acid	7.36	$C_{24}H_{36}O_2$	M + H	357.2805	5	94.5
27	HMDB0030539	Tangeritin	9.34	$C_{20}H_{20}O_7$	M + H	373.1314	9	85.0
28	HMDB0013627	Cervonoyl ethanolamide	6.96	$C_{24}H_{36}O_3$	M + H	373.2754	4	88.9
29	HMDB0029540	Nobiletin	7.24	$C_{21}H_{22}O_8$	M + H	403.1418	8	91.7
30	HMDB0015698	Cinitapride	16.44	$C_{21}H_{30}N_4O_4$	M + H	403.235	3	95.8
31	HMDB0030404	Armillaripin	14.32	$C_{24}H_{30}O_6$	M + H	415.2132	4	100.0
32	HMDB0035728	Ganoderol A	17.55	$C_{30}H_{46}O_2$	M + H	439.3606	8	91.3
33	HMDB0011133	DHAP (18:0)	11.99	$C_{21}H_{41}O_7P$	M + NH4	454.2928	0	88.9
34	HMDB0031958	3-O-Acetylepisamarcandin	10.42	$C_{26}H_{34}O_6$	M + NH4	460.2703	2	95.5
35	HMDB0010382	LysoPC (16:0/0:0)	12.12	$C_{24}H_{50}NO_7P$	M + H	496.3399	0	82.6
36	HMDB0010408	LysoPC (P-18:1(9Z)/0:0)	14.72	$C_{26}H_{52}NO_6P$	M + H	506.3615	2	100
37	HMDB0012108	LysoPC (17:0/0:0)	13.4	$C_{25}H_{52}NO_7P$	M + H	510.3558	1	100
38	HMDB0010384	LysoPC (18:0/0:0)	14.73	$C_{26}H_{54}NO_7P$	M + H	524.3709	0	81.7
39	HMDB0011496	LysoPE (0:0/22:6(4Z,7Z,10Z,13Z,16Z,19Z))	11.13	$C_{27}H_{44}NO_7P$	M + H	526.2946	3	100
40	HMDB0010393	1-Meadoyl-sn-glycero-3-phosphocholine	11.22	$C_{28}H_{52}NO_7P$	M + H	546.3552	0	100
41	HMDB0010392	LysoPC (20:2(11Z,14Z)/0:0)	13.46	$C_{28}H_{54}NO_7P$	M + H	548.3702	2	100
42	HMDB0010404	LysoPC (22:6(4Z,7Z,10Z,13Z,16Z,19Z)/0:0)	11.23	$C_{30}H_{50}NO_7P$	M + H	568.3421	4	100
43	HMDB0008070	PC (18:1(11Z)/18:1(11Z))	17.22	$C_{44}H_{84}NO_8P$	M + H	786.6041	4	100
44	HMDB0008377	PC (20:3(5Z,8Z,11Z)/20:3(8Z,11Z,14Z))	28.98	$C_{48}H_{84}NO_8P$	M + H	834.6048	5	97.1

observed. No such inflammation was observed in the OVX + QEP group (Figure 10(A–C)). Serum TNF-α, IL-6 and IFN-γ levels were significantly higher in the OVX group than in the SHAM group. QEP can regulate serum IL-6 and TNF-α levels after modelling, whereas IFN-γ did not exhibit any significant differences (Figure 10(D–F)).

Quantification of SCFAs in faecal samples

As shown in Table 10, acetate acid, propionate acid and butyrate acid were the three most abundant SCFAs in rat faeces. Compared with those in rats of the SHAM group, the concentrations of acetate and propionate were decreased in rats of the OVX groups. This result indicated that the function of the gut microbiota is influenced by the OVX operation. Also, QEP could regulate the content of acetate, propionate and butyrate in rat faeces.

Discussion

Numerous studies have indicated that PMO is highly related to the constituents of the gut microbiota (Dao et al. 2016). QEP has been reported to play a critical role in bone metabolism,

although the mechanism of action remains to be explored (Shuai et al. 2019). In this study, we evaluated the effects of QEP on the gut microbiota of OVX rats. Our results suggest that QEP affects bone metabolism by restoring the constituents of the intestinal flora community. Specifically, QEP can regulate gut microbiota dysbiosis in OVX rats, it can regulate the content of inflammatory factors and repair the damaged intestinal barrier, and it can regulate the contents of SCFAs in the intestinal environment of OVX rats.

Furthermore, QEP can affect special sequences of β collagen in blood markers, which are related to bone metabolism, such as β-cross laps, N-terminal osteocalcin and total procollagen type N-terminal propeptide. QEP also affects the mRNA expression of vitamin D receptors in OVX rats, thereby effectively controlling osteoporosis (Shuai et al. 2014). In this study, OVX rats exhibited remarkable osteoporotic changes in bone microstructure, including decreased BMD, BV/TV, BS/TV and Tb.N, and increased Tb.Sp. Decreased oestrogen levels in OVX rats lead to significant alteration of the microstructure of cancellous bones, which is characterized by the conversion of plate-like trabeculae to rod-like structures. This can increase trabecular separation and reduce the number of trabecular bones. Treatment with QEP can significantly alleviate these alterations in the bone

Table 7. Identification results of endogenous metabolites in rat plasma that are meaningful for grouping under negative ion mode.

No.	Database ID	Identification	Retention	Formula	Adduct	Extract mass	Delta (ppm)	Matching rate
1	HMDB0000929	L-Tryptophan	2.14	$C_{11}H_{12}N_2O_2$	M–H	203.0833	3	100
2	HMDB0014457	Pentobarbital	5.32	$C_{11}H_{18}N_2O_3$	M–H	225.1251	3	93.2
3	HMDB0000827	Stearic acid	23.07	$C_{18}H_{36}O_2$	M–H	283.2648	2	100
4	HMDB0014607	Sodium tetradecyl sulphate	22.43	$C_{14}H_{30}O_4S$	M–H	293.1781	4	100
5	HMDB0001043	Arachidonic acid	18.48	$C_{20}H_{32}O_2$	M–H	303.2338	3	100
6	HMDB0032549	N-Undecylbenzenesulfonic acid	16.7	$C_{17}H_{28}O_3S$	M–H	311.168	2	97.2
7	HMDB0004626	Tetrahydrogestrinone	15.09	$C_{21}H_{28}O_2$	M–H	311.2017	0	100
8	HMDB0031031	2-Dodecylbenzenesulfonic acid	21.21	$C_{18}H_{30}O_3S$	M–H	325.184	1	95
9	HMDB0002183	Docosahexaenoic acid	18.08	$C_{22}H_{32}O_2$	M–H	327.2334	1	98.1
10	HMDB0035676	1-Hydroxy-1-phenyl-3-hexadecanone	20.43	$C_{22}H_{36}O_2$	M–H	331.2649	2	100
11	HMDB0000268	Tetrahydrocorticosterone	6.57	$C_{21}H_{34}O_4$	M–H	349.2385	0	100
12	HMDB0000277	Sphingosine 1-phosphate	9.24	$C_{18}H_{38}NO_5P$	M–H	378.241	1	97
13	HMDB0000619	Cholic acid	6.96	$C_{24}H_{40}O_5$	M–H	407.2805	0	100
14	HMDB0011503	LysoPE (16:0/0:0)	11.98	$C_{21}H_{44}NO_7P$	M–H	452.2792	2	100
15	HMDB0035353	Epoxyganoderiol C	17.57	$C_{30}H_{48}O_3$	M–H	455.3529	0	100
16	HMDB0012496	1-Lyso-2-arachidonoyl-phosphatidate	17.32	$C_{23}H_{39}O_7P$	M–H	457.2364	1	100
17	HMDB0000138	Glycocholic acid	5.61	$C_{26}H_{43}NO_6$	M–H	464.3	4	100
18	HMDB0010381	LysoPC (15:0/0:0)	14.1	$C_{23}H_{48}NO_7P$	M–H	480.3097	0	100
19	HMDB0010382	LysoPC (16:0/0:0)	13.4	$C_{24}H_{50}NO_7P$	M–H	494.3234	4	100
20	HMDB0011481	LysoPE (0:0/20:0)	14.71	$C_{25}H_{52}NO_7P$	M–H	508.3417	2	100
21	HMDB0002639	Sulfolithocholylglycine	4.76	$C_{26}H_{43}NO_7S$	M–H	512.2683	1	100
22	HMDB0011496	LysoPE (0:0/22:6(4Z,7Z,10Z,13Z,16Z,19Z))	11.07	$C_{27}H_{44}NO_7P$	M–H	524.2796	3	100
23	HMDB0011493	LysoPE (0:0/22:4(7Z,10Z,13Z,16Z))	11.2	$C_{27}H_{48}NO_7P$	M–H	528.3108	2	100
24	HMDB0011499	LysoPE (0:0/24:6(6Z,9Z,12Z,15Z,18Z,21Z))	11.17	$C_{29}H_{48}NO_7P$	M–H	552.3115	4	100
25	HMDB0240261	1-Stearoylglycerophosphoinositol	28.97	$C_{27}H_{53}O_{12}P$	M–H	599.3212	2	100
26	HMDB0009256	PE (20:1(11Z)/18:1(11Z))	19.8	$C_{43}H_{82}NO_8P$	M–H	770.5712	1	100
27	HMDB0009585	PE (22:4(7Z,10Z,13Z,16Z)/18:0)	18.13	$C_{45}H_{82}NO_8P$	M–H	794.569	2	96.1
28	HMDB0009815	PI (18:0/20:4(5Z,8Z,11Z,14Z))	14.22	$C_{47}H_{83}O_{13}P$	M–H	885.5548	6	100
29	HMDB0004891	Ganglioside GA2 (d18:1/18:0)	14.71	$C_{56}H_{104}N_2O_{18}$	M–H	1091.726	4	100

Table 8. Identification results of potential biomarkers of osteoporosis.

No.	Metabolites	Formula	Pathway	HMDB ID	KEGG ID	PUBCHEM
1	Glycocholic acid	$C_{26}H_{43}NO_6$	H	HMDB0000138	C01921	23617285
2	Tetrahydrocorticosterone	$C_{21}H_{34}O_4$	G	HMDB0000268	C05476	9863245
3	Sphinganine	$C_{18}H_{39}NO_2$	A	HMDB0000269	C00836	91486
4	Sphingosine 1-phosphate	$C_{18}H_{38}NO_5P$	A	HMDB0000277	C06124	5353956
5	17a-Hydroxypregnenolone	$C_{21}H_{32}O_3$	G	HMDB0000363	C05138	91451
6	Cholic acid	$C_{24}H_{40}O_5$	H	HMDB0000619	C00695	221493
7	L-Tryptophan	$C_{11}H_{12}N_2O_2$	K	HMDB0000929	C00078	6305
8	Arachidonic acid	$C_{20}H_{32}O_2$	D,I	HMDB0001043	C00219	444899
9	alpha-Linolenic acid	$C_{18}H_{30}O_2$	J	HMDB0001388	C06427	5280934
10	Corticosterone	$C_{21}H_{30}O_4$	G	HMDB0001547	C02140	5753
11	Docosahexaenoic acid	$C_{22}H_{32}O_2$	I	HMDB0002183	C06429	445580
12	Phytosphingosine	$C_{18}H_{39}NO_3$	A	HMDB0004610	C12144	122121
13	9E,11E-Octadecadienoic acid	$C_{18}H_{32}O_2$	B,I	HMDB0005047	C04056	5282796
14	11-cis-Retinol	$C_{20}H_{30}O$	C	HMDB0006216	C00899	5280382
15	PC (18:1(11Z)/18:1(11Z))	$C_{44}H_{84}NO_8P$	B,D,E,J	HMDB0008070	C00157	24778895
16	PC (20:3(5Z,8Z,11Z)/20:3(8Z,11Z,14Z))	$C_{48}H_{84}NO_8P$	B,D,E,J	HMDB0008377	C00157	53478975
17	LysoPC (20:2(11Z,14Z))	$C_{28}H_{54}NO_7P$	B,D,E,J	HMDB0010392	C04230	52924053
18	LysoPC (22:6(4Z,7Z,10Z,13Z,16Z,19Z))	$C_{30}H_{50}NO_7P$	B,D,E,J	HMDB0010404	C04230	10415542
19	1-lyso-2-Arachidonoyl-phosphatidate	$C_{23}H_{39}O_7P$	D,I	HMDB0012496	NA	53481443

microstructure of OVX rats. The results of this study demonstrate that QEP can inhibit the development of osteoporosis in OVX rats.

Recently, the gut microbiota has attracted the attention of many researchers because it is associated with metabolic diseases. The human gastrointestinal tract is colonized by rich and dynamic microbial communities. These microbes have been considered a critical factor for metabolic disorders, including obesity, diabetes and osteoporosis (Ejtahed et al. 2016). Thus, they provide a potential method for the diagnosis and treatment of metabolic disorders (Steves et al. 2016). In addition to the immune system, the gut microbiota also affects metabolism and intestinal barrier function. Finally, intestinal microbes affect the process of osteoporosis by affecting drug metabolism or via other pathways (Ke et al. 2019). TCM, which typically contains a complex of compound components, is commonly administered orally.

Although its bioavailability is low, it often shows satisfactory curative effects in clinics. This may be partially caused by gut microbiota. Generally, glycosides contained in TCM are poorly absorbed in the intestine. Due to their low bioavailability, glycosides remain in the intestinal tract for quite a long time. After being metabolized by the intestinal flora, they are mainly absorbed in the form of aglycones (Zheng et al. 2018). Our results showed that QEP can regulate the composition of the gut microflora community in OVX rats. The level of Firmicutes in OVX rats was significantly higher than that in SHAM rats. This result is consistent with that of osteoporosis patients (Yatsonsky et al. 2019). After QEP treatment, the increase in Firmicutes was reversed. Firmicutes play an important role in absorbing calories from the diet and storing fat in cells of the gut tract. In OVX rats, the increased F/B ratio suggests that micro-ecological disorders occur in intestinal microbes (Zhang et al. 2018). Studies

Table 9. Mass spectrum response intensity results of biomarkers in each group of plasma.

Metabolites	SHAM	OVX	OVX + QEP
Sphinganine	138309.00 ± 6744.78	97056.17 ± 22274.59**	141025.50 ± 9526.83##
17a-Hydroxypregnenolone	24448.17 ± 3624.71	335.00 ± 167.34**	1853.67 ± 1783.68#
Arachidonic acid	306021.17 ± 40505.10	162345.17 ± 21232.51**	267945.17 ± 17032.68##
alpha-Linolenic acid	122533.83 ± 20912.51	54490.83 ± 7114.61**	85953.50 ± 23057.84*,##
Corticosterone	34397.00 ± 12407.63	84034.33 ± 9170.16**	46131.50 ± 2809.61*,##
Docosahexaenoic acid	200855.33 ± 10616.66	91945.50 ± 11379.02**	163005.00 ± 39315.98*,##
Phytosphingosine	205007.17 ± 18840.63	137923.33 ± 11720.77**	214333.50 ± 16804.79##
9E,11E-Octadecadienoic acid	300927.83 ± 37838.00	145755.00 ± 10282.14**	206023.33 ± 23495.15**,##
11-cis-Retinol	32096.50 ± 6220.81	14648.33 ± 2081.33**	25166.83 ± 2598.00*,##
PC (18:1(11Z)/18:1(11Z))	27435.67 ± 3313.67	18857.83 ± 5389.77**	27542.50 ± 1595.79##
PC (20:3(5Z,8Z,11Z)/20:3(8Z,11Z,14Z))	5557.83 ± 506.47	2482.67 ± 319.42**	5257.00 ± 825.42##
LysoPC (20:2(11Z,14Z)/0:0)	88605.50 ± 11896.04	45743.50 ± 6386.17**	61193.50 ± 6905.02**,##
LysoPC (22:6(4Z,7Z,10Z,13Z,16Z,19Z)/0:0)	866379.33 ± 135683.28	443690.33 ± 67149.98**	473418.33 ± 53589.55**
L-Tryptophan	305551.00 ± 21872.06	219563.67 ± 27319.04**	270166.83 ± 25780.81*,##
Tetrahydrocorticosterone	67802.50 ± 11770.13	6035.83 ± 1400.48**	10816.67 ± 7143.64**
Sphingosine 1-phosphate	45182.67 ± 7678.10	28745.33 ± 11038.43*	33012.83 ± 5462.94*
Cholic acid	61178.33 ± 36634.00	873.00 ± 282.77**	19495.00 ± 8953.54*,##
1-lyso-2-Arachidonoyl-phosphatidate	16361.33 ± 3276.19	9079.00 ± 1251.38**	12387.50 ± 6344.67
Glycocholic acid	20080.83 ± 4372.29	607.67 ± 148.67**	4475.50 ± 644.57**,##

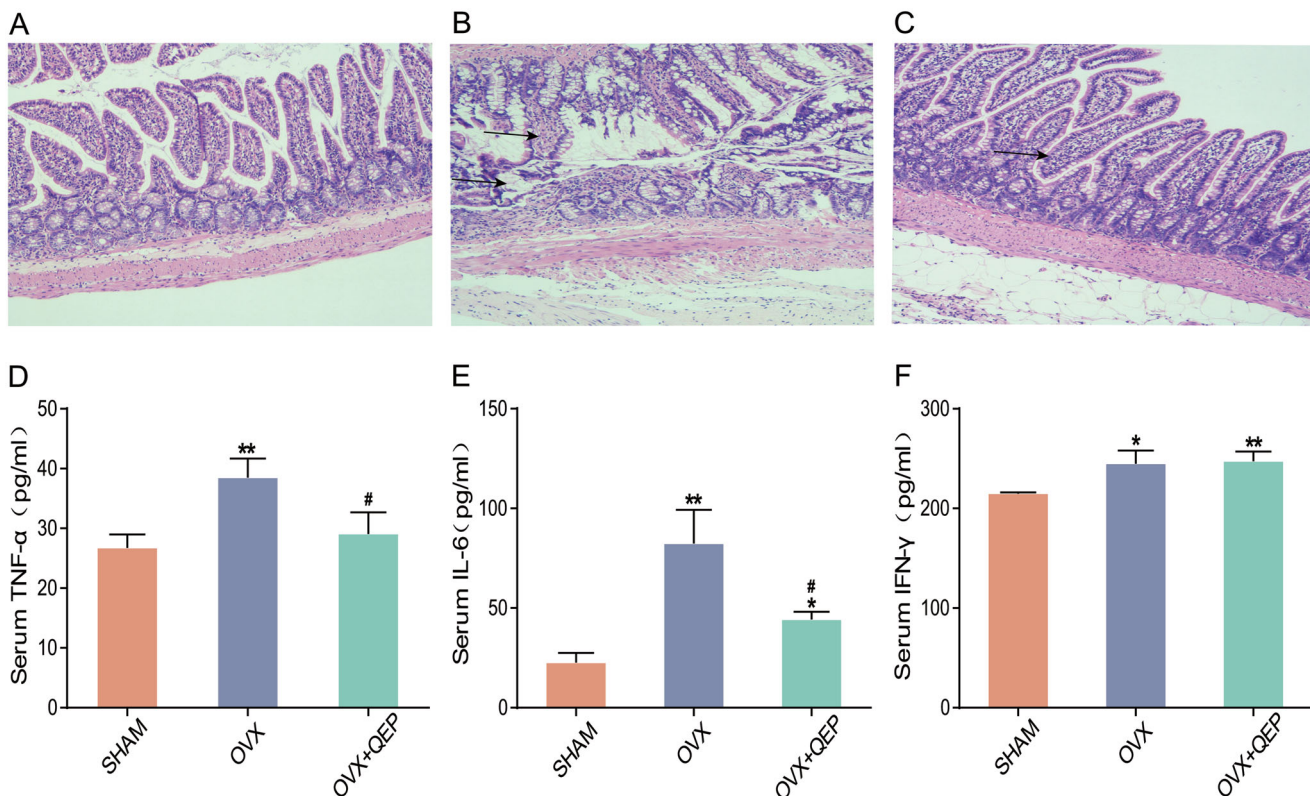*$p < 0.05$ vs. SHAM; **$p < 0.01$; #$p < 0.05$ vs. OVX; ##$p < 0.01$.

Figure 10. QEP regulates the intestinal barrier and serum levels of TNF-α, IL-6 and IFN-γ in OVX rats. (a–c) H&E staining (original magnification, ×100). (d–f) Serum levels of TNF-α, IL-6 and IFN-γ. The data are expressed as means ± SD ($n = 6$ in each group). *$p < 0.05$ vs. SHAM; **$p < 0.01$. #$p < 0.05$ vs. OVX.

Table 10. QEP regulates SCFAs.

	SHAM	OVX	QEP
Acetic acid	378.10 ± 58.49	271.95 ± 52.41**	447.73 ± 46.54*,###
Propionic acid	48.48 ± 11.45	28.96 ± 5.73**	53.41 ± 14.26##
Butyric acid	29.74 ± 13.76	24.92 ± 18.97	67.78 ± 35.68*,#
Valeric acid	5.99 ± 1.19	5.48 ± 0.76	5.92 ± 0.71
Isobutyric acid	4.00 ± 2.30	2.30 ± 0.59	3.48 ± 1.67
Isovaleric acid	0.93 ± 0.70	0.86 ± 0.40	1.21 ± 0.71

*$p < 0.05$ vs. SHAM; **$p < 0.01$. #$p < 0.05$ vs. OVX; ##$p < 0.01$; ###$p < 0.001$.

have demonstrated that an increased proportion of Firmicutes induces immune responses, including the activation of Th17 cells (Kim et al. 2012; Magrone and Jirillo 2013). Th17 cytokines, such as IL-17, can induce RANKL expression and osteoclastogenesis (Kim et al. 2015).

In this study, the level of *Lactobacillus* was significantly reduced in the OVX group compared to that in the SHAM group. After QEP treatment, the abundance of *Lactobacillus* in the OVX + QEP group was significantly increased. Thus, QEP can regulate the abundance of *Lactobacillus*, which plays an important role in the prevention of bone loss. Probiotics have been investigated for their ability to treat osteoporosis (Zhang et al. 2015). *Lactobacillus* is one of the most important probiotics used in the regulation of BMD in both animal models and

humans. Schepper et al. (2020) found that the abundance of Verrucomicobiales and Bacteriodales phyla in the intestinal microbiota of male C57/Bl6J mice treated with glucocorticoids (GC-Tx) for 8 weeks was altered. *Lactobacillus reuteri* (Lactobacillaceae) was successfully used to prevent trabecular bone loss in GC-Tx mice. Liu et al. (2019) found that *Lactobacillus rhamnosus* GG protected against tenofovir-induced mandibular bone loss in mice by rescuing mesenchymal stem cells proliferation and osteogenesis. Schepper et al. (2019) presented evidence that dysbiosis-induced bone loss can be prevented by treatment with *L. reuteri* by enhancing the intestinal barrier function. Thus, the gut microbiota-bone axis must be considered when treating osteoporosis.

In addition to *Lactobacillus*, changes in several other intestinal microorganisms were observed. Several metabolic processes in the ileum, as well as immunological processes in both the ileum and colon, were affected by *Akkermansia muciniphila* (Verrucomicrobiaceae) (Benthe et al. 2018). The content of *A. muciniphila* is a marker of the health status of gut microbiota. *A. muciniphila* can maintain the integrity of the intestinal barrier in mice, as demonstrated in diet-induced obese animal models (Benthe et al. 2019). Furthermore, *A. muciniphila* is involved in immune regulation and the enhancement of trans-epithelial resistance. The latter activity is achieved by modulating the expression of tight junction proteins (Plovier et al. 2017). In addition, *A. muciniphila* reduces systemic inflammation by improving intestinal wall integrity, thus leading to the reduction of circulating lipopolysaccharide (Chelakkot et al. 2018). *Blautia* is a Gram-positive, anaerobic bacterium belonging to the Lachnospiraceae family, and it participates in the development of disturbances in glucose metabolism (Kashtanova et al. 2018). A recent study showed that *Blautia* may significantly activate the secretion of TNF-α (Egshatyan et al. 2016). Zhu et al. (2020) found that increased levels of *Blautia* were positively correlated with inflammatory indicators, such as IL-1β, TNF-α and IL-6. Furthermore, *Blautia* produces butyric acid (Zhai et al. 2020).

Colonization of Firmicutes and increased diversity of intestinal microbes are associated with increased inflammatory response in the gut tract. Increased inflammation is correlated with osteoclast activation at the bone site. Gut-mediated inflammation is characterized by the expression of TNF-α, IL-1 and IL-6. They play important roles in osteoclast activation and sustained osteoporosis (Yatsonsky et al. 2019).

SCFAs are metabolites of gut microbiota. They serve as a link between microbiota and host homeostasis and play an important role in the regulation of inflammation and the metabolism of glucose and lipids. SCFAs are beneficial in modulating energy homeostasis, lipid metabolism and appetite regulation (Schoeler and Caesar 2019). Acetic acid and propionic acid are the two main products of Bacteroidetes, whereas butyric acid is mainly produced by Firmicutes (Chakraborti 2015). Studies have revealed that butyric acid can upregulate vitamin D receptors and regulate proteins associated with calcium absorption (Xu et al. 2017). Activation of the butanoate metabolism pathway corresponds to increased relative abundances of Firmicutes (Liu et al. 2014; Vemuri et al. 2018). In this study, the relative abundance of Firmicutes was higher in OVX rats than in SHAM. This result corroborates the stronger butanoate metabolism in OVX rats, although the mechanism of the microbiota effects on butanoate metabolism remains unclear. Further investigation is needed to reveal the relationships among microbiota, butanoate metabolism and calcium absorption.

Conclusions

QEP is a promising option for the treatment of PMO and the regulation of gut microbiota may be a potential therapeutic strategy for osteoporosis. Our results demonstrated that QEP improved osteoporotic bone microstructure in OVX rats. This may be caused by the regulation of the gut microbiota composition. The mechanism of action partially entails the upregulation of probiotics. However, more in-depth exploration is required to determine how and to what extent the anti-osteoporotic effects of QEP are correlated with the regulation of gut microbiota.

Disclosure statement

The authors declare that there are no conflicts of interest associated with this publication.

ORCID

Hui Xie http://orcid.org/0000-0002-8083-4616

References

Benthe VDL, Rusli F, Lute C, Lamprakis A, Salazar E, Boekschoten MV, Hooiveld GJ, Müller M, Vervoort J, Kersten S, et al. 2018. Integrative analysis of gut microbiota composition, host colonic gene expression and intraluminal metabolites in aging C57BL/6J mice. Aging. 10(5):930–950.

Benthe VDL, van Beek AA, Aalvink S, Meijer B, Sovran B, Vermeij WP, Brandt RMC, Savelkoul HFJ, Steegenga WT, Belzer C. 2019. Akkermansia muciniphila ameliorates the age-related decline in colonic mucus thickness and attenuates immune activation in accelerated aging mice. Immun Ageing. 16:6.

Chakraborti CK. 2015. New-found link between microbiota and obesity. World J Gastrointest Pathophysiol. 6(4):110–119.

Chelakkot C, Choi Y, Kim DK, Park HT, Ghim J, Kwon Y, Jeon J, Kim MS, Jee YK, Gho YS, et al. 2018. Akkermansia muciniphila-derived extracellular vesicles influence gut permeability through the regulation of tight junctions. Exp Mol Med. 50(2):e450.

Dao MC, Everard A, Aron-Wisnewsky J, Sokolovska N, Prifti E, Verger EO, Kayser BD, Levenez F, Chilloux J, Hoyles L, et al. 2016. Akkermansia muciniphila and improved metabolic health during a dietary intervention in obesity: relationship with gut microbiome richness and ecology. Gut. 65(3):426–436.

Egshatyan L, Kashtanova D, Popenko A, Tkacheva O, Tyakht A, Alexeev D, Karamnova N, Kostryukova E, Babenko V, Vakhitova M, et al. 2016. Gut microbiota and diet in patients with different glucose tolerance. Endocr Connect. 5(1):1–9.

Ejtahed HS, Soroush AR, Angoorani P, Larijani B, Hasani-Ranjbar S. 2016. Gut microbiota as a target in the pathogenesis of metabolic disorders: a new approach to novel therapeutic agents. Horm Metab Res. 48(6):349–358.

Feng WC, Jin LP, Li HL, Hu H, Wang WM. 2014. Research progress of intestinal flora on the metabolic mechanism of effective components of traditional Chinese medicine. Heilongjiang J Tradit Chin Med. 43:90–92.

Hamm AK, Manter DK, Kirkwood JS, Wolfe LM, Cox-York K, Weir TL. 2019. The effect of hops (Humulus lupulus L.) extract supplementation on weight gain, adiposity and intestinal function in ovariectomized mice. Nutrients. 11(12):3004.

Kashtanova DA, Tkacheva ON, Doudinskaya EN, Strazhesko ID, Kotovskaya YV, Popenko AS, Tyakht AV, Alexeev DG. 2018. Gut microbiota in patients with different metabolic statuses: Moscow Study. Microorganisms. 6(4):98.

Ke K, Arra J, Abu-Amer Y. 2019. Mechanisms underlying bone loss associated with gut inflammation. Int J Mol Sci. 20:4323.

Kim KA, Gu W, Lee IA, Joh EH, Kim DH. 2012. High fat diet-induced gut microbiota exacerbates inflammation and obesity in mice via the TLR4 signaling pathway. PLoS One. 7(10):e47713.

Kim KW, Kim HR, Kim BM, Cho ML, Lee SH. 2015. Th17 Cytokines regulate osteoclastogenesis in rheumatoid arthritis. Am J Pathol. 185(11): 3011–3024.

Liu G, Fang T, Yan T, Jia G, Zhao H, Huang Z, Chen X, Wang J, Xue B. 2014. Metabolomic strategy for the detection of metabolic effects of spermine supplementation in weaned rats. J Agric Food Chem. 62(36): 9035–9042.

Liu H, Gu R, Li W, Xue J, Cong Z, Wei Q, Zhou Y. 2019. Probiotics protect against tenofovir-induced mandibular bone loss in mice by rescuing mandible-derived mesenchymal stem cell proliferation and osteogenic differentiation. J Oral Rehabil. 47:1–8.

Liu L, Zhu XY, Lu JL. 2018. Effect of salt processing on the dissolution of main components of Qing'e Pills. Chin Patent Med. 40:2714–2718.

Lucas S, Omata Y, Hofmann J, Böttcher M, Iljazovic A, Sarter K, Albrecht O, Schulz O, Krishnacoumar B, Krönke G, et al. 2018. Short-chain fatty acids regulate systemic bone mass and protect from pathological bone loss. Nat Commun. 9(1):55.

Magrone T, Jirillo E. 2013. The interaction between gut microbiota and age-related changes in immune function and inflammation. Immun Ageing. 10(1):31.

Pacifici R. 2012. Role of T cells in ovariectomy induced bone loss-revisited. J Bone Miner Res. 27(2):231–239.

Plovier H, Everard A, Druart C, Depommier C, Van HM, Geurts L, Chilloux J, Ottman N, Duparc T, Lichtenstein L, et al. 2017. A purified membrane protein from Akkermansia muciniphila or the pasteurized bacterium improves metabolism in obese and diabetic mice. Nat Med. 23(1): 107–113.

Rios-Arce ND, Collins FL, Schepper JD, Steury MD, Raehtz S, Mallin H, Schoenherr DT, Parameswaran N, McCabe LR. 2017. Epithelial barrier function in gut-bone signaling. Adv Exp Med Biol. 1033:151–183.

Saleh N, Nassef NA, Shawky MK, Elshishiny MI, Saleh HA. 2020. Novel approach for pathogenesis of osteoporosis in ovariectomized rats as a model of postmenopausal osteoporosis. Exp Gerontol. 137:110935.

Schepper JD, Collins F, Rios-Arce ND, Kang HJ, Schaefer L, Gardinier JD, Raghuvanshi R, Quinn RA, Britton R, Parameswaran N, et al. 2020. Involvement of the gut microbiota and barrier function in glucocorticoid-induced osteoporosis. J Bone Miner Res. 35(4):801–820.

Schepper JD, Collins FL, Rios-Arce ND, Raehtz S, Schaefer L, Gardinier JD, Britton RA, Parameswaran N, McCabe LR. 2019. Probiotic Lactobacillus reuteri prevents postantibiotic bone loss by reducing intestinal dysbiosis and preventing barrier disruption. J Bone Miner Res. 34(4):681–698.

Schoeler M, Caesar R. 2019. Dietary lipids, gut microbiota and lipid metabolism. Rev Endocr Metab Disord. 20(4):461–472.

Shoback D, Rosen CJ, Black DM, Cheung AM, Murad MH, Eastell R. 2019. Pharmacological management of osteoporosis in postmenopausal women: an Endocrine Society* Clinical Practice Guideline. J Clin Endocrinol Metab. 104(5):1595–1622.

Shuai B, Yang YP, Shen L, Ke H. 2014. Effects of Qing'e formula on the expression of bone metabolic markers and VDR mRNA in postmenopausal osteoporosis patients. Chin Med. 5(3):145–152.

Shuai B, Zhu R, Yang YP, Shen L, Xu XJ, Ma C, Lu L. 2019. Positive effects of Qing'e Pills on trabecular microarchitecture and its mechanical properties in osteopenic ovariectomised mice. Chin J Integr Med. 25(4):270–277.

State Pharmacopoeia Committee. 2015. Pharmacopoeia of the People's Republic of China: one [S]. Beijing: Chemical Industrial Press; p. 1024.

Steves CJ, Bird S, Williams FM, Spector TD. 2016. The microbiome and musculoskeletal conditions of aging: a review of evidence for impact and potential therapeutics. J Bone Miner Res. 31(2):261–269.

Tyagi AM, Yu M, Darby TM, Vaccaro C, Li J-Y, Owens JA, Hsu E, Adams J, Weitzmann MN, Jones RM, et al. 2018. The microbial metabolite butyrate stimulates bone formation via T regulatory cell-mediated regulation of WNT10B expression. Immunity. 49(6):1116–1131.

Vemuri R, Shinde T, Gundamaraju R, Gondalia SV, Karpe AV, Beale DJ, Martoni CJ, Eri R. 2018. Lactobacillus acidophilus DDS-1 modulates the gut microbiota and improves metabolic profiles in aging mice. Nutrients. 10(9):1255.

Wang Y, Yao J, Cai L, Liu T, Wang X, Zhang Y, Zhou Z, Li T, Liu M, Lai R, et al. 2020. Bone-targeted extracellular vesicles from mesenchymal stem cells for osteoporosis therapy. Int J Nanomedicine. 15:7967–7977.

Xie G, Zhang S, Zheng X, Jia W. 2013. Metabolomics approaches for characterizing metabolic interactions between host and its commensal microbes. Electrophoresis. 34(19):2787–2798.

Xu X, Jia XY, Mo L, Liu C, Zheng L, Yuan Q, Zhou X. 2017. Intestinal microbiota: a potential target for the treatment of postmenopausal osteoporosis. Bone Res. 5:17046.

Yan CP, Weng ZB, Wu Y, Chen ZP, Cai BC, Li WD. 2014. Comparative study on anti-ovariectomized osteoporosis effect of Qing'e Pills and raw drugs. J Nanjing Univ Chin Med. 30:438–442.

Yatsonsky ID, Pan K, Shendge VB, Liu J, Ebraheim NA. 2019. Linkage of microbiota and osteoporosis: a mini literature review. World J Orthop. 10(3):123–127.

Zhai SS, Ruan D, Zhu YW, Li MC, Ye H, Wang WC, Yang L. 2020. Protective effect of curcumin on ochratoxin A-induced liver oxidative injury in duck is mediated by modulating lipid metabolism and the intestinal microbiota. Poult Sci. 99(2):1124–1134.

Zhang J, Motyl KJ, Irwin R, MacDougald OA, Britton RA, McCabe LR. 2015. Loss of bone and Wnt10b expression in male type 1 diabetic mice is blocked by the probiotic Lactobacillus reuteri. Endocrinology. 156(9): 3169–3182.

Zhang Q, Yu H, Xiao X, Hu L, Xin F, Yu X. 2018. Inulin-type fructan improves diabetic phenotype and gut microbiota profiles in rats. PeerJ. 6: e4446.

Zheng H, Wei QM, Jiang JL, Xie TT, Su ZH. 2018. Research progress on interaction between traditional Chinese medicine and intestinal flora. Chin Folk Med. 27:58–62.

Zhu L, Sha L, Li K, Wang Z, Wang T, Li Y, Liu P, Dong X, Dong Y, Zhang X, et al. 2020. Dietary flaxseed oil rich in omega-3 suppresses severity of type 2 diabetes mellitus via anti-inflammation and modulating gut microbiota in rats. Lipids Health Dis. 19(1):20.

Zu XP, Lin Y, Xie HS, Yang N, Liu XR, Zhang WD. 2016. Research progress on the interaction between active ingredients of traditional Chinese medicine and intestinal flora. China J Chin Mater Med. 41:1766–1772.